Analytical Approximation to the Scheutjens−Fleer Theory for Polymer Adsorption from Dilute Solution. 1. Trains, Loops, and Tails in Terms of Two Parameters: The Proximal and Distal Lengths

G. J. Fleer* and J. van Male

Laboratory for Physical and Colloid Science, Agricultural University, Wageningen, Dreijenplein 6, 6703 HB Wageningen, The Netherlands

A. Johner

Institut Charles Sadron, 6 rue Boussingault, 67083 Strasbourg Cedex, France

Received May 19, 1998; Revised Manuscript Received November 10, 1998

ABSTRACT: Recently an analytical self-consistent mean-field theory was proposed for homopolymer adsorption in the long-chain limit. Here we make direct contact between that formalism and the numerical lattice model of Scheutjens and Fleer. The lattice layer closest to the wall is treated in a discrete manner, whereas a continuum description is used further out. This entails a new boundary condition at the wall. Together with the self-consistency condition, this leads to two equations from which the two relevant length scales (the proximal and distal lengths) follow unambiguously. As a result, analytical solutions in closed form are obtained for both (mean-field) good solvents (from $\chi = 0$ up to $\chi \approx 0.47$) and a Θ solvent ($\chi = 0.5$). For good solvents the agreement between the full lattice calculation and the analytical model is excellent; for a Θ solvent the discrepancy can amount to about 10%. The approximations necessary to render the analytical problem tractable are carefully checked against the numerical data.

1. Introduction

The topic of polymer adsorption has a long history in colloid science and polymer physics. The experimental interest derives from the many possibilities in which macroscopic and colloidal surfaces may be modified by polymers. In the colloidal domain, polymers are widely used to stabilize or destabilize colloidal particles, to improve or inhibit the deposition of particles on macroscopic surfaces, and to obtain the desired rheological behavior of colloidal dispersions.[1] In all these situations the behavior of the interfacial polymer layers is of crucial importance.

From a theoretical point of view, the problem is intriguing because the presence of the surface affects the conformational properties of the polymer chains drastically. Several theoretical models have been proposed. An overview can be found in a recent monograph.[2] One of the models that has been rather successful is the numerical self-consistent-field (SCF) model proposed by Scheutjens and Fleer.[2−4] It can describe, on a mean-field level, a wide variety of interfacial polymer layers. An obvious drawback of any numerical model is that it is not easy to recognize general trends (such as the dependence of the adsorbed amount and layer thickness on parameters such as the chain length, the solution concentration, the solvency, and the segmental adsorption energy). So far, no quantitative equations in closed form are available for describing the numerical SCF results. An earlier attempt by Ploehn et al.[5,6] was only partially successful. Their derivation yielded a less tractable and less physical form of the boundary condition at the solid surface and neglected excluded-volume interactions between tails and loops. These points affect the results both qualitatively and quantitatively.

Along quite different lines, a number of coarse-grained models have been developed to interpret such general trends. A famous example is the scaling analysis as pioneered by De Gennes.[7] This treatment relies on a rather general argument. In the plateau regime, the adsorption layer has locally the structure of a semidilute solution characterized by the correlation length of concentration fluctuations ξ, which is proportional to a power of the local concentration φ: $\xi \propto \varphi^{-\alpha}$. The exponent α is unity at the Θ-point and is smaller in a good solvent: in that case $\alpha = {}^1/_2$ in mean field and $\alpha = {}^3/_4$ when excluded-volume statistics are assumed. In the absence of any other length scale, ξ is proportional to the distance z from the wall, and the concentration in the layer decays as the power law $\varphi \propto z^{-1/\alpha}$. This power law describes the whole layer in the academic limit of infinite chain length at vanishing concentration. For finite chain lengths a characteristic length d enters, which can be viewed upon as the layer thickness. We will also refer to it as the distal length; a precise definition will be given later. With the assumption that d is the only intrinsic length, the scaling prediction is $\varphi \propto d^{-1/\alpha} f(z/d)$, where the scaling function f has the limiting behaviors $f(x) \propto x^{-1/\alpha}$ for $x \to 0$ and $f(x) \propto e^{-x}$ for $x \to \infty$. There is also a lower cutoff length (or proximal length) p, which is of the order of the monomer size and which is mainly determined by the monomer/wall interaction. For the power law to be observed over a significant range, the two cutoff lengths p and d must be well separated.

About 5 years ago, Van der Linden and Leermakers[8] tried to compare the scaling predictions to numerical SCF results for very long chains (up to 10^5 segments per chain, which corresponds to molar masses of order 10 million) and found indeed similarities for those extreme conditions. However, chains this long hardly occur in practice.

De Gennes' argument does not depend on the detailed layer structure in terms of trains, loops, and tails; as

10.1021/ma980793y CCC: $18.00
Published on Web 02/09/1999

such it does not make any prediction on this structure (though the neglect of tails gives direct access to the loop size distribution $P(s) \sim s^{-11/5}$ necessary to construct the power law profile with $\alpha = {}^3/_4$; see also Appendix II of the second paper in this series). To this end the ϕ^4 field theory[9] can be used, on account of the analogy with critical phenomena first pointed out by De Gennes. This approach does not explicitly account for tail monomers but predicts a power-law decrease for the distribution of chain ends. Tail monomers can only be reintroduced as a perturbation from the predicted chain-end concentration, which fails in the outer part of the layer for very long chains at moderate dilution.[10] Very recently, Aubouy et al.[11] augmented the scaling analysis by a free energy functional approach, allowing to describe the loop and tail size distributions; this approach has been applied to various systems. The obtained end-point distribution close to the wall is qualitatively different from the field-theory prediction, but the model has the appeal of simplicity. In the following we will argue that for reasonable chain lengths and/or high dilution the neglect of tails as compared to loops only fails in the dilute edge of the layer, where the physics are anyhow dominated by the cutoff length d and not by the local concentrations.[12] This is the basis of our analytical approximation to the mean-field theory.

Over the past few years, Semenov et al.[13] developed an elegant analytical mean-field treatment for adsorption of homopolymers from a good solvent. The starting point is a ground-state approximation (GSA) for loops, but they were also able to account for tails. The contribution of tails is given by a product of the ground-state eigenfunction (the square of which gives the loop concentration) and another function accounting for free chain ends. For both functions a differential equation was formulated; both are defined in terms of two parameters (length scales), the *proximal length* p and the *distal length* d referred to above. In the formalism of Semenov et al. for dilute solutions, p is determined by the adsorption strength and d is proportional to (but smaller than) the radius of gyration of the chains; the proportionality factor depends mainly on the bulk solution concentration. For $p \ll d$, which is typical for strong adsorption of extremely long chains from dilute solutions, there is a region in the adsorbed layer (the so-called central region) where De Gennes' scaling laws apply. In the more common situation where the length scales p and d are not well separated, such a central regime is nearly absent, even in the plateau regime. In the starved Henry regime, which can be described with the same differential equations, again two parameters p and d occur, but now $p \gg d$. The length d retains the same meaning (exponential cutoff, layer thickness), but p (which enters as an integration constant) loses its meaning of proximal length: one relevant length scale d (which now depends only on the adsorption energy) is sufficient to describe the exponential decay in this regime.

The theory of Semenov et al.[13] represents the long-chain asymptotics of the continuum mean-field theory (for example, the adsorbance is expanded up to $N^{-2/3}$ terms). After the introduction of dimensionless variables, the problem is reduced to determining the appropriate numerical functions. However, the scales in different regions of the layer are not the same. Semenov et al. define a length scale z^* separating an inner layer made up by loops and an outer layer where tails dominate; they assume $z^* < d$. The equations for the central regime ($p < z < d$) are then governed by z^*, while in those for the distal regime ($z > d$) only d occurs. The solutions are asymptotically matched, which is only accurate if the length scales are well separated.[13] For shorter chains, typically up to 10^4 segments, which are most relevant for experiments, one can write explicit solutions that are rather accurate over the whole layer, as shown by Johner et al.[12] In that case z^* is larger than d, and z^* does not enter the equations since in the tail-dominated regime the physics are determined by the exponential cutoff d.

In the present paper we elaborate this continuum formalism of ref 12 and establish a direct connection with the discrete equations used in the numerical SCF lattice model. We explicitly formulate two equations from which the lengths p and d may be determined. The first is the condition of conservation of end points (also called the self-consistency condition) and expresses the fact that the number of end points is twice the number of chains, and the number of adsorbed chains is directly related to the adsorbance in trains, loops, and tails. This condition was also used by Semenov et al.[13] In the plateau region of the adsorption isotherm, it gives the equation from which the distal length d may be found. The second equation is the boundary condition at the surface, for which we formulate a direct link between the continuum and lattice models; in the plateau region it directly provides p as a function of the adsorption strength. More generally, the two equations referred to above constitute a set of two simultaneous equations, which can be solved for the two unknown parameters p and d. This generalized treatment includes the plateau region (where the two equations can be uncoupled) but describes the undersaturated Henry region as well (with the proviso that the mean-field approach has its shortcomings for describing the dilute surface regime). In contrast to the boundary condition classically used in continuum theories, the constraint of an impenetrable wall is strictly fulfilled. Therefore, there is a (nonuniversal) adsorption threshold in the theory (though in mean field subtle critical surface effects are lost, such as the weak divergence of the concentration profile at the wall). Our treatment also allows to account for strong interactions in the very vicinity of the wall, and the surface concentration nicely saturates in the strong adsorption limit (far from the adsorption threshold). As the result, a rather accurate approximation of the numerical SCF model for homopolymer adsorption for a wide range of conditions is obtained (for universal as well as nonuniversal properties), both for good solvents and for a Θ solvent.

The paper is organized as follows. In section 2, we give a summary of the relevant SCF equations as used in the lattice model. In section 3 we describe in general terms the continuum model as introduced by Semenov et al.,[13] and we derive their two differential equations by rewriting the discrete propagator relation in the lattice model in a continuum version. Moreover, we formulate the two equations to determine p and d. In section 4, we give explicit approximate solutions for both good solvents and a Θ solvent in terms of p and d. Finally, in section 5 we check the fundamental assumptions in the analytical model against the full numerical SCF computations, and we make a first comparison between the two models. In the second paper of this series, we compare in more detail the predictions for a

variety of structural details of the adsorbed layer.

Appendix I gives a list of the most important symbols used in this paper.

2. Exact Lattice SCF

In this section we summarize the most important equations of the self-consistent-field (SCF) theory, which is exact within the limits of a mean-field lattice model. Each chain is subdivided into segments with ranking number $s = 1, 2, \ldots N$, and these segments can take only discretized positions with respect to the surface, in lattice layers numbered $z = 1, 2, \ldots$. The spacing l between the lattice layers is equal to the bond length a when a simple cubic lattice (with lattice parameter $\lambda = {}^1/_6$) is used. For other lattice types $l \neq a$. For example, in a hexagonal lattice ($\lambda = {}^1/_4$), l is the height of regular tetrahedron with edge a: $l = a\sqrt{4/6}$ or $l = a/\sqrt{6\lambda}$. For convenience, in this paper we express all distances in units of l. We have to realize, however, that, whereas the length a is invariant in different lattices, l is not: its value should be adjusted to λ according to $l = a/\sqrt{6\lambda}$, keeping the bond length constant.

An important quantity is the *end-point distribution* $G_{z,s}$, which is the weight of all possible walks of s segments ($s - 1$ steps) ending in layer z. Its value for $s = N$ is related to the volume fraction φ_z^{e} of chain ends according to

$$\varphi_z^{\mathrm{e}} = 2\varphi_{z,N} = \frac{2\varphi^{\mathrm{b}}}{N} G_{z,N} \tag{1}$$

where $\varphi^{\mathrm{b}} = \varphi_\infty$ is the bulk solution volume fraction of segments and $\varphi_{z,N}$ is the volume fraction of end segments ($s = N$) in layer z. Obviously, $\varphi_{\infty,N} = \varphi^{\mathrm{b}}/N$ in the bulk solution, where $G_{\infty,s} = 1$ for any s. An equivalent formulation of this latter statement is setting the field u_∞ in the bulk solution equal to zero.

In the continuum description, to be discussed in section 3, the end-point distribution is denoted as $G(z,s)$, where z is now a continuous variable (with the surface situated at $z = 0$) and s runs along the contour of the chain from zero to N. This contour may be chopped up into N sections of one bond length each, which may be seen as the segments in the discrete model. The mapping of $G_{z,s}$ (lattice) and $G(z,s)$ (continuum) will be done by a shift over half a lattice layer: $G_{1,s} = G({}^1/_2,s)$ since adsorbed segments are in the first (surface) layer of the lattice ($z = 1$), and their center in the continuum model is at $z = {}^1/_2$. Thus, we will identify $G_{z,s}$ with $G(z - {}^1/_2,s)$.

In the lattice model, the end-point distribution $G_{z,s}$ in a field u_z is computed from a recurrence (propagator) relation which may be written as[2,3]

$$\mathrm{e}^{u_z} G_{z,s+1} = G_{z,s} + \lambda(G_{z-1,s} - 2G_{z,s} + G_{z+1,s}) \tag{2}$$

where, as discussed above, the lattice parameter λ is equal to ${}^1/_6$ in a simple cubic lattice and to ${}^1/_4$ in a hexagonal lattice. We note that the continuum version of the term in brackets is $\partial^2 G(z,s)/\partial z^2$. With the starting condition

$$G_{z,0} = 1 \quad \text{or} \quad G_{z,1} \equiv G_z = \mathrm{e}^{-u_z} \tag{3a,b}$$

the end-point distribution $G_{z,s}$ in a specified field u_z may be computed for any z and s. For the quantity $G_{z,1}$, which gives the distribution of monomers in the field u_z but which is also the *segment weighting factor* for a chain segment in layer z, we use the abbreviated symbol G_z.

In the polymer adsorption problem, u_z is not a fixed imposed field, but it is affected by the accumulation of segments near the surface. Therefore, it is a function of the segment volume fraction profile $\{\varphi_z\}$ which, in turn, is a function of the entire set $\{G_{z,s}\}$: the field is self-consistent. This self-consistent field $u(\{\varphi_z\})$ may, in an extended Flory−Huggins model, be written as[2,3]

$$u_z = -(\chi_s + \lambda\chi)\delta_{z-1} - 2\chi(\langle\varphi_z\rangle - \varphi^{\mathrm{b}}) - \ln\left(\frac{1-\varphi_z}{1-\varphi^{\mathrm{b}}}\right) \tag{4}$$

where χ_s is the adsorption energy parameter and χ the Flory−Huggins solvency parameter. As anticipated above $u_\infty = 0$ (or $G_\infty = 1$). The Kronecker delta δ_{z-1} is unity for $z = 1$ and zero elsewhere: only adsorbed segments experience the adsorption energy (and the missing fraction λ of solute contacts which give rise to an energetic contribution unless $\chi = 0$). The angular brackets represent local plus nonlocal effects: $\langle\varphi_z\rangle$ is defined as $\varphi_z + \lambda(\varphi_{z-1} - 2\varphi_z + \varphi_{z+1}) \approx \varphi + \lambda\, \mathrm{d}^2\varphi/\mathrm{d}z^2$. The terms "local" (contributions due to layer z only) and "nonlocal" (with also contributions from the neighboring layers) are used here in the same sense as introduced by Helfand[15] and by Hong and Noolandi.[16] In the continuum approach we will neglect nonlocal effects in the energy part of u and identify $\langle\varphi_z\rangle$ with φ_z for $z > 1$. For $\chi = 0$ this has no consequences as the nonlocal energy contribution vanishes. However, for a Θ solvent (where in eq 4 the term linear in φ cancels if $\langle\varphi_z\rangle$ is replaced by φ_z) the nonlocal effect is relatively much more important. For example, in the power-law regime $\varphi \propto z^{-1}$ in a Θ solvent, the correction amounts to $2\lambda/z^2$ as compared to one, which may be significant in the inner layers. It has been shown[2] that the nonlocal energy term, which is a second derivative $\mathrm{d}^2\varphi/\mathrm{d}z^2$ in the field u, leads to a square gradient contribution $(\mathrm{d}\varphi/\mathrm{d}z)^2$ in the interfacial free energy.[24]

Equation 4 shows how u_z, to be used in eq 2, depends on φ_z. In turn, φ_z may be expressed in u_z and $\{G_{z,s}\}$, which constitutes the closure relation in the SCF equations. For $\varphi(\{u_z\})$ we have the so-called composition law[2,3,5]

$$\varphi_{z,s} = \frac{\varphi^{\mathrm{b}}}{N} \mathrm{e}^{u_z} G_{z,s} G_{z,N-s+1} \qquad \varphi_z = \sum_{s=1}^{N} \varphi_{z,s} \tag{5a,b}$$

showing that $\varphi_{z,s}$ is computed from combining two walks (from either chain end) toward segment s in layer z. The factor e^{u_z} in eq 5a corrects for the double counting of segment s. Equation 5a for $s = N$ reduces to eq 1. The set of eqs 2−5 can, in general, only be solved numerically.

The above equations give the overall distribution of all chains, both adsorbed and free. To extract more structural information on adsorbed chains, G can be separated into a contribution G^{a} due to adsorbed chains and a part G^{f} due to free chains:

$$G_{z,s} = G^{\mathrm{a}}_{z,s} + G^{\mathrm{f}}_{z,s} \tag{6}$$

Both G^{a} and G^{f} satisfy the propagator relation 2. However, the starting conditions for G^{a} and G^{f} are different. For G^{f} we can still use $G^{\mathrm{f}}_{z,0} = 1$, as in eq 3a, but in addition $G^{\mathrm{f}}_{1,s}$ has to be set zero for any s. For G^{a}

we have $G^{a}_{z,1} = e^{-u_z}\delta_{z-1}$ (so that G_1 is the only nonzero element of G_z) and $G^{a}_{1,s} = G_{1,s}$.

Substitution of eq 6 into eq 5 gives the contributions of trains (tr), loops (l), and tails (t) of adsorbed chains and that of free chains (f): $\varphi_1 = \varphi^{tr}$, $\varphi_z = \varphi^{l}_z + \varphi^{t}_z + \varphi^{f}_z$ for $z > 1$. Train and loop segments form the connection between two adsorbed sequences, tail segments that between a free and an adsorbed chain section, and segments in free chains connect two free walks. The various contributions are thus given by[2−4]

$$\varphi^{trl}_z = \frac{\varphi^{b}}{N} e^{u_z} \sum_{s=1}^{N} G^{a}_{z,s} G^{a}_{z,N-s+1} \tag{7a}$$

$$\varphi^{t}_z = \frac{2\varphi^{b}}{N} e^{u_z} \sum_{s=1}^{N} G^{f}_{z,s} G^{a}_{z,N-s+1} \tag{7b}$$

$$\varphi^{f}_z = \frac{\varphi^{b}}{N} e^{u_z} \sum_{s=1}^{N} G^{f}_{z,s} G^{f}_{z,N-s+1} \tag{7c}$$

where φ^{trl} is the concentration of trains and loops, with $\varphi^{tr} = \varphi^{trl}_1$ and $\varphi^{l}_z = \varphi^{trl}_z$ for $z > 1$.

Analogously to eq 1, the end-point distribution φ^{ae}_z of adsorbed chains is given by

$$\varphi^{ae}_z = 2\varphi^{a}_{z,N} = \frac{2\varphi^{b}}{N} G^{a}_{z,N} \tag{8}$$

Whereas $\varphi^{e}_\infty = 2\varphi^{b}/N$ and $G_{\infty,N} = 1$ (eq 1), $\varphi^{ae}_\infty = 0$ and $G^{a}_{\infty,N} = 0$ since the bulk solution contains only free chains. The number of adsorbed chains (per lattice site) equals half the number of end points per lattice site (hence, it equals $\sum_z \varphi^{a}_{z,N}$). This number is Γ/N, where Γ is the adsorbance (in equivalent monolayers):

$$\Gamma = \varphi^{b} G^{a}_{N} \qquad G^{a}_{N} = \sum_z G^{a}_{z,N} \tag{9a,b}$$

Obviously, Γ can also be obtained as $\Gamma^{tr} + \Gamma^{l} + \Gamma^{t}$, where

$$\Gamma^{tr} = \varphi_1 \qquad \Gamma^{l} = \sum_z \varphi^{l}_z \qquad \Gamma^{t} = \sum_z \varphi^{t}_z \tag{10a,b,c}$$

In the exact SCF equations, both pathways to calculate Γ give identical results: the self-consistency condition that the number of end points is twice the number of chains (which is equivalent to the conservation of end points) is automatically obeyed.

3. Continuum Approximation

3.1. General. For weak variations in the field (i.e., not too close to the surface), the discrete propagator relation (eq 2) may be transformed into a differential equation. The difference $e^{u_z}G_{z,s+1} - G_{z,s}$ may then be written as $(e^{u_z\Delta s}G_{z,s+\Delta s} - G_{z,s})/\Delta s$ (with $\Delta s = 1$ in the lattice version), which for $\Delta s \to 0$ becomes $\partial G(z,s)/\partial s + u(z)G(z,s)$, where $G(z,s)$ and $u(z)$ are now continuous functions. Adsorbed segments will be treated as discrete species (occupying the region $0 < z < 1$), with their center at $z = {}^1/_2$. As mentioned before, when comparing continuous and lattice equations, we will identify $G_{z,s}$ with $G(z - {}^1/_2,s)$ and u_z with $u(z - {}^1/_2)$, where z is a positive integer. The last term in eq 2 approaches $\lambda\, \partial^2 G/\partial z^2$, which we abbreviate as $\lambda G''$. We note that this is the appropriate expression when z is taken in units of the lattice spacing l. When z is a real distance, the term $\lambda G''$ is thus $\lambda l^2 \partial^2 G/\partial z^2$, which is identical to $(a^2/6)\partial^2 G/\partial z^2$ as commonly used in continuum models, because l equals the bond length a divided by $\sqrt{6\lambda}$ (see the discussion above eq 1).

Hence, the continuum version of eq 2 is

$$\lambda G'' = \partial G/\partial s + uG \tag{11}$$

with the boundary condition $G(z,0) = 1$, analogously to eq 3. For the boundary condition at the surface we have to define $G(0,s)$. In our approach to the problem, $G(0,s)$ is replaced by $G({}^1/_2,s)$, which will be treated separately below (section 3.4). Only in this boundary condition does the adsorption energy χ_s enter. In formulating this condition, we make a connection between the lattice and continuum descriptions by treating the train layer discretely, whereas in the remainder of the adsorbed layer the continuum description is maintained. We choose this procedure because the continuum model is expected to break down on length scales of a segment size or below. In this respect, our treatment of the continuum model differs from that of Semenov et al.[13] and Ploehn et al.[5,6]

Exact analytical solutions for eq 11 with a fully self-consistent field u have not been found. The standard procedure to determine the end-point distribution in a given field is an eigenfunction expansion $G(z,s) = \sum_k \psi_k(z) e^{\epsilon k s}$. These eigenfunctions are determined by eq 11 supplemented by the proper boundary conditions. When the eigenvalues $-\epsilon_k$ are well separated, G is dominated by the lowest eigenvalue $-\epsilon$, the ground-state eigenvalue; for adsorbing chains in the plateau region ϵ is a positive (small) number which, however, should be larger than $1/N$.[13] In this so-called ground-state approximation (GSA), the variables z and s are thus separated by writing $G(z,s) = \psi(z)e^{\epsilon s}$, where $\psi(z)$ is the ground-state eigenfunction. However, in the adsorption problem the situation is very different for configurations that touch (G^{a}) or do not touch (G^{f}) the wall. Due to the attractive wall/monomer potential, there is a bound state with an energy $-\epsilon$ which dominates G^{a}, whereas there is no bound state entering the expansion of G^{f}.

The constant ϵ is, in general, a function of N, φ^{b}, and χ_s; it has to be determined from the boundary condition at the surface and/or the conservation of end points. This parameter ϵ often occurs in the combination $\varphi^{b}e^{\epsilon N}$, for which we introduce a separate symbol:

$$b^2 = \varphi^{b} e^{\epsilon N} \qquad \epsilon = \epsilon_0 + \frac{2}{N} \ln b \qquad \epsilon_0 = \frac{1}{N} \ln\left(\frac{1}{\varphi^{b}}\right) \tag{12a,b,c}$$

We will see that b^2 is of order φ_1. In the plateau region of the adsorption isotherm b is thus of order (but below) unity. Then the logarithmic term in eq 12b constitutes only a small correction and $\epsilon \approx \epsilon_0$ as defined in eq 12c; the parameter ϵ_0 is only a function of N and φ^{b} and is small for long chains. In dilute solutions ($\varphi^{b} \ll 1$) in the plateau region the condition $\epsilon > 1/N$ is thus satisfied. In the undersaturated Henry region of the adsorption isotherm (extremely low φ^{b}), b^2 is still of order φ_1 but now $\varphi^{b} \ll \varphi_1 \ll 1$. Now $\epsilon \approx N^{-1} \ln(\varphi_1/\varphi^{b})$ may be of order unity and is only a function of χ_s. In this Henry region $\varphi^{b} \ll e^{-\epsilon N}$.

Since in this standard GSA all segments are considered to be "middle segments", end effects are ne-

glected: tails cannot be described. A better approximation was introduced by Semenov et al.[13] They write $G = G^a + G^f$, which is the same as eq 6 in lattice SCF. In the lattice version, G^a and G^f obey the same recurrence relation, though with different boundary conditions. The same holds in the continuum approach, where now eq 2 is replaced by the diffusion-type eq 11. As explained before, on the basis of an expansion for high chain lengths, the GSA approach is still used, but only for G^a. We return to this point in the next section.

To make progress, the field u in eq 11 has to be specified. A suitable starting point is eq 4 for $z > 1$. The value of u_1, which contains χ_s, will be incorporated in the boundary condition (section 3.4). If we consider only dilute solutions (small φ^b) and expand the logarithm, we have from eq 4

$$u(z) \approx v\varphi + \frac{1}{2}\varphi^2 - 2\lambda\chi\frac{d^2\varphi}{dz^2} \quad (z > 1) \tag{13}$$

where $v \equiv 1 - 2\chi$ is Edwards' excluded-volume parameter. Equation 13 shows that $u \approx v\varphi$ in good solvents (i.e., solvents in which the second virial term $v\varphi$ dominates) and $u \approx {}^1/_2\varphi^2$ in a Θ solvent (where the linear term cancels because $\chi = 0.5$). These approximations imply the neglect of nonlocal energy effects (i.e., the last term of eq 13); only for $\chi = 0$ this has no consequences as the nonlocal term vanishes. As discussed earlier,[24] the lattice theory accounts for these effects in a model-dependent way. We shall see later that the neglect of nonlocality in the analytical treatment is relatively inaccurate close to the surface, but it makes the analytical model easier without dramatic consequences.

To solve eq 11 or its simpler GSA variant (eq 15 below), we will need a relation between φ and G (or ψ).

3.2. Trains and Loops. As stated above, we use GSA for G^a. For convenience, we renormalize the eigenfunction ψ and define a function g by $g(z) = b\psi(z)$ so that

$$G^a(z,s) = b^{-1}g(z)e^{\epsilon s} \tag{14}$$

Substitution of this result in eq 11 for G^a gives a differential equation in g:

$$\lambda g'' = (\epsilon + u)g \tag{15}$$

where g, which depends only on z, specifies the end-point distribution (see eq 18 below), and g^2 is related to the segment concentration in trains and loops. This can be seen by inserting eq 14 into eq 7a: $\varphi^{trl}(z) = e^{u(z)}g^2(z)$, since the factor $b^{-2}\varphi^b e^{\epsilon N}$ is unity on account of eq 12a. The factor $e^{u_z} = 1/G_z$ in this expression is necessary in the discrete model in order to prevent double counting the weighting factor G_z of the joining segment of two walks ending at this segment (see eq 5a). In the continuum approach, we neglect this factor and use the simple relation

$$\varphi^{trl} \approx g^2 \tag{16}$$

The difference between the two models is expected to be most pronounced in the few layers next to the surface layer (say, layers 2−5); in these layers e^{u_z} may be of order 1.1−1.2 (or even higher for short chains). In the surface layer the factor e^{u_1} will be taken into account through the boundary condition (section 3.4); in the layers further out $e^{u_z} \approx 1$ so that this correction is then irrelevant. Note that it is the renormalization $g = b\psi$ which enables us to write φ^{trl} (and thus φ^{tr} and φ^l) simply as the square of the eigenfunction g.

According to eq 13, $u \approx v\varphi$ or $u \approx {}^1/_2\varphi^2$, depending on the solvency. Here, $\varphi = \varphi^{trl} + \varphi^t + \varphi^f$. Over most of the adsorbed layer φ^f can be neglected. Also the contribution of φ^t in the sum $\epsilon + u$ is small. In the inner layers $\varphi^t \ll \varphi^{trl}$, and further out $\varphi^t \ll \epsilon$. The latter condition is equivalent to the statement that z^*, which separates the loop-dominated and tail-dominated regimes, is larger than $d = \sqrt{\lambda/\epsilon}$ (see also eq 30), so that d is the only relevant length scale. For extremely long chains ($N \gg 10^4$) a situation might occur where $z^* < d$; then z^* would enter the equations. We do not consider such long chains.

Only in the region where φ^t reaches its maximum may an appreciable error occur if we neglect the contribution of tails to the field altogether. We expect to get a reasonable estimate for g, with probably the right trends, if we use $\varphi = \varphi^{trl}$ in u, which results in

$$\lambda g'' = (\epsilon + vg^2)g \quad \text{(good solvents)} \tag{17a}$$

$$\lambda g'' = (\epsilon + {}^1/_2\, g^4)g \quad (\Theta \text{ solvent}) \tag{17b}$$

The solution of these equations will be given in section 4.2. They are written in terms of two parameters. The first, obviously, is ϵ, which is related to the exponential cutoff length d through $\epsilon = \lambda/d^2$. In the plateau regime d may also be called the *distal length*. The second is a length p, which enters as an integration constant: if $g(z)$ satisfies eq 17a or 17b, $g(z + p)$ is a solution as well. In the plateau regime p may be named the *proximal length*, which is then directly related to the extrapolation length, defined as the inverse of $-[d \ln g/dz]_{z=0}$.[17] The extrapolation length is the length obtained when the tangent at $z = 0$ of the plot of g against z is extrapolated toward the abscissa axis.

For determining the two parameters p and d, we need two equations. These are the boundary condition at the surface, and the self-consistency condition for the conservation of end points and will be given in section 3.4.

The end-point distribution $\varphi^{ae}(z)$ is found by substituting eq 14 into eq 8, which results in $\varphi^{ae} = (2/N)bg$ since again $\varphi^b e^{\epsilon N} = b^2$. Moreover, $\Gamma = (N/2)\sum_z \varphi^{ae} = b\sum_z g$. We split the sum in the discrete part $0 < z < 1$ (for the train layer) where we use $g_1 = g({}^1/_2)$, and the region $z > 1$ (loops and tails) where we replace the summation by an integration. Hence,

$$\varphi^{ae} = \frac{2b}{N}g \tag{18}$$

$$\Gamma = b(g_1 + I_g) \qquad I_g \equiv \int_1^\infty g\, dz \tag{19a,b}$$

Equation 19a expresses the conservation of end points. To find an expression for b, Γ has to be written as a sum over trains, loops, and tails. For trains and loops the function g contains all the information, but for tails we need a second function f.

3.3. Tails. In the previous section it was shown that the loop concentration can be approximated as the square of g, which follows from eq 7a: $\varphi^l(z) \propto G^a(z,s)\, G^a(z,N - s)$. Equation 7b shows that all terms contributing to the tail profile φ^t are proportional to the product of $G^a = b^{-1}ge^{\epsilon s}$ and G^f. This suggests that φ^t could be

written as a product of two functions g and f, where f is connected to G^f. In fact, $f(z)$ can be defined as the ratio between $\varphi^t(z)$ and $\varphi^{ae}(z)$:

$$\varphi^t = \varphi^{ae} f = \frac{2b}{N} gf \qquad (20a,b)$$

where in eq 20b we used eq 18 for φ^{ae}. From eqs 7b and 8 we have

$$f_z = \frac{e^{u_z}}{G^a_{z,N}} \sum_{s=1}^{N} G^f_{z,s}\, G^a_{z,N-s+1} \quad f(z) \approx \int_0^N G^f(z,s) e^{-\epsilon s}\, ds \qquad (21a,b)$$

Equation 21b was obtained by substituting $G^a = b^{-1} g e^{\epsilon s}$ (eq 14) into eq 21a, neglecting again the factor e^u. This equation was first derived by Semenov et al.[13] For long chains the upper integration limit may be taken as infinity. The boundary condition $G^f_{1,s} = 0$ in the lattice model may be translated into $G^f_{(1,s)} = 0$: hence, $f(1) = 0$ because the train layer ($0 < z < 1$) is forbidden for tails and free chains. For large z, where $G^f = 1$, f reaches a constant level: $f(\infty) = 1/\epsilon$.

The quantity $G^f(z,s)$ satisfies the diffusion-type eq 11. This enables us to find a differential equation for f, by multiplying eq 11 for G^f with $e^{-\epsilon s}$ and integrating over s. The term $\int(\partial G^f/\partial s) e^{-\epsilon s} ds$ can be evaluated by partial integration and gives $-1 + \epsilon f$, where the term -1 originates from $[G^f e^{-\epsilon s}]_0^\infty = -1$ on account of the boundary constraint $G^f(z,0) = G(z,0) = 1$. Hence, f satisfies the differential equation

$$1 + \lambda f'' = (\epsilon + u) f \qquad (22)$$

with $f(1) = 0$. Because of the similar structures of the differential eqs 15 and 22, f can be computed from g (which is known after solving eq 17). After Johner et al.[12] the following relation holds:

$$\lambda f = \alpha_1 g + \alpha_2 g_0 \qquad (23)$$

where the functions α_1, α_2, and g_0 can be computed from g according to

$$g_0 = g \int g^{-2}\, dz \quad d\alpha_1/dz = g_0 \quad d\alpha_2/dz = -g \qquad (24a,b,c)$$

Equation 23 can be verified by differentiating this equation twice with respect to z and substituting the result into $\lambda f g'' = g(1 + \lambda f'')$, which relation follows from eqs 15 and 22.

3.4. Conservation of End Points and Boundary Condition. Once g and f are known, the adsorbed layer characteristics can be calculated. As stated above, g contains two parameters: ϵ (or d) and p. Since f is computed from g, no new parameters occur. We need two equations to determine these two parameters. The first is found from the conservation of end points (eq 19a), using $\Gamma = \Gamma^{tr} + \Gamma^l + \Gamma^t$. These contributions may be expressed in g and f by integrating eqs 16 and 20:

$$\Gamma^{tr} = g_1^2 \quad \Gamma^l = I_{gg} \quad \Gamma^t = \frac{2b}{N} I_{gf} \qquad (25a,b,c)$$

where the integrals I_{gg} and I_{gf} are defined analogously to eq 19b:

$$I_{gg} = \int_1^\infty g^2\, dz \quad I_{gf} = \int_1^\infty gf\, dz \qquad (26a,b)$$

Combining eqs 19a and 25 gives an expression for b. Together with eq 12a this provides the final equation for the conservation of end points:

$$\epsilon N = \ln\left(\frac{1}{\varphi^b}\right) + 2 \ln b \quad b = \frac{g_1^{\,2} + I_{gg}}{g_1 + I_g - (2/N) I_{gf}} \qquad (27a,b)$$

Quite often, we will replace ϵ by λ/d^2 (where d is the exponential cutoff length, see eq 30) and $\ln(1/\varphi^b)$ by y^2 (see eq 29), where y is a convenient concentration parameter in dilute solutions.

The second equation, giving the boundary condition at the surface, follows from the recurrence relation 2 for $z = 1$, using again eq 14 for $G(z,s)$. We will identify $G(z,s)$ for $z = {}^1/_2$ and ${}^3/_2$ with $G^a(z,s)$, which is exact for the surface layer and introduces no appreciable error for the second layer. As before, we have $g_1 = g({}^1/_2)$ for the surface layer and $g_2 = g({}^3/_2)$ for the second layer. The result is

$$\epsilon + u_1 = \ln\left(\lambda_0 + \lambda \frac{g_2}{g_1}\right)$$
$$u_1 = -(\chi_s + \lambda\chi) - 2\chi(\lambda_0 g_1^{\,2} + \lambda g_2^{\,2}) - \ln(1 - g_1^{\,2}) \qquad (28a,b)$$

where eq 28b follows from eq 4 with $\langle\varphi_1\rangle = \lambda_0 g_1^2 + \lambda g_2^2$. In these equations, we use the abbreviation $\lambda_0 \equiv 1 - 2\lambda$. Since we are interested mainly in dilute solutions, we neglect φ^b in eq 4. As compared to u for $z > 1$ (eq 13), there are three differences: (i) for adsorbed segments the adsorption energy enters, (ii) since $\varphi_1 = g_1^2$ may be high, we do not expand the logarithm in eq 28b, and (iii) for the surface layer we account for nonlocal effects (i.e., we distinguish between $\langle\varphi_1\rangle$ and φ_1).

Equations 27 and 28 enable us to find p and d as a function of N, φ^b, and χ_s. In general, the two simultaneous equations have to be solved numerically for p and d. However, there are two important limiting cases where the equations can be uncoupled. In the plateau regime and for long chains, g_1 and g_2 in eq 28 turn out to be only a function of p (see sections 4.3.2 and 4.3.3), so that when $\epsilon \ll u_1$ this equation then immediately gives p. On the other hand, in the Henry regime the ratio g_2/g_1 depends only on d (see section 4.3.1), and because $u_1 \approx -\chi_s - \lambda\chi$ in this regime, eq 28a may be solved for d as the only unknown. Once p and d are known, the functions g and f, which contain all the information about the adsorbed layer characteristics, can be computed, as shown in the following section.

4. Explicit Expressions for Good Solvents and a Θ Solvent

4.1. General. So far, we have discussed adsorbed layer properties in terms of g and f without specifying the form of these functions. To be able to use the equations derived above, we need explicit expressions. These depend on the relation between u and g and thus on the solvency. The starting points are eq 17a for good solvents and eq 17b for a Θ solvent. We present the solutions in terms of a concentration parameter y, a distal length d, a proximal length p, and a reduced

distance x. As we will see, the terms "distal" and "proximal" are appropriate for the plateau regime, but not for the Henry regime.

The parameter y is defined by

$$y^2 = \ln(1/\varphi^b) \tag{29}$$

and enables us to write eq 12c as $\epsilon_0 = y^2/N$.

The "distal" length d specifies the exponential decay length of g far from the surface. The high z limit of eqs 17a and 17b reads $\lambda g'' = \epsilon g$, or $g'' = d^{-2}g$, so that g is proportional to $e^{-z/d}$, where

$$d = \sqrt{\frac{\lambda}{\epsilon}} \quad \frac{1}{d^2} = \frac{1}{{d_0}^2} + \frac{2}{\lambda N}\ln b \quad d_0 = \sqrt{\frac{\lambda}{\epsilon_0}} = \frac{\sqrt{\lambda N}}{y} = \frac{R}{y} \tag{30a,b,c}$$

Equation 30 may be compared with eq 12. In eqs 30b and 30c, the parameter $d_0 = \sqrt{\lambda/\epsilon_0}$ is a first-order estimate for d in the plateau region, and in eq 30c R is the radius of gyration, equal to $\sqrt{\lambda N}$ lattice spacings l (which is the same as $\sqrt{N/6}$ bond lengths a because $l = a/\sqrt{6\lambda}$). According to eq 30c, the distal length d in dilute solutions is considerably smaller than the radius of gyration R. This corresponds to $\epsilon N \approx y^2 \gg 1$, which is a prerequisite of the present treatment.[13] In the Henry regime, the second term in eq 30b, which is roughly equal to $(\lambda N)^{-1} \ln \varphi_1$, is no longer small. This equation may be rewritten as $\lambda/d^2 \approx N^{-1} \ln(\varphi_1/\varphi^b)$, which in the Henry regime turns out to be only a function of χ_s. The length d is then the only relevant length scale, is no longer "distal", and depends only on χ_s.

As mentioned before, the length p is an integration constant in the differential eqs 17a and 17b. For the plateau regime, p is smaller than d and may be called "proximal" length; it is then directly related to the extrapolation length $-[\mathrm{d}z/\mathrm{d}\ln g]_{z=0}$. In the Henry regime, where p is larger than d, the latter length takes over the function of extrapolation length and p loses its meaning.

Once a form for $g(z)$ is found in terms of p and d, we can substitute $g_1 = g(1/2)$, $g_2 = g(3/2)$, and the integrals I_g, I_{gg}, and I_{gf} into eqs 27 and 28 and find p and d from these two equations.

Finally, the reduced distance x is defined by $x = (z + p)/d$. The parameter x is thus measured in units of d, and its value at the surface ($z = 0$) is $x_0 = p/d$.

For the mapping of continuum and lattice equations, we need the value of x at $z = 1/2$, 1, and $3/2$. Hence, we define

$$x = \frac{z+p}{d} \quad x_i = \frac{p_i}{d} \quad p_i = p + \frac{i}{2} \tag{31a,b,c}$$

Clearly, $i = 1$ refers to the middle of the train layer (first layer), $i = 2$ to the boundary of the first and second layers (which is the lower bound of the continuum region), and $i = 3$ to the middle of the second layer (from which loops and tails start). Tails and free chains can only visit the region $x > x_2$ ($z > 1$).

In the following sections, we first discuss good solvents and then a Θ solvent ($\chi = 0.5$).

4.2. The Functions *g* and *f*. 4.2.1. *Good Solvents.* The differential eq 17a has the solution $g = 2\sqrt{\epsilon/\nu}/\sinh[\sqrt{\epsilon/\lambda}(z + p)]$, where p is an integration constant. In terms of d (eq 30) and x (eq 31a), we write

$$g = \frac{\sqrt{2\lambda/\nu}}{d \sinh x} \tag{32}$$

The function $g(z)$ is sketched in Figure 1, both with a linear and with a logarithmic scale for z.

Equation 32 and Figure 1 show, for the case $p \ll d$ and a good solvent, the well-known characteristic features in the proximal ($z \lesssim p$), central ($p \ll z \ll d$), and distal ($z \gg d$) regions as discussed by De Gennes:[7,17] g is of order $\sqrt{2\lambda}/p$ in the proximal region (more precisely, its value is $\sqrt{2\lambda}/p_1$ in the middle of the train layer); it follows approximately the mean-field power law $g \propto z^{-1}$ in the central region, and it decays exponentially ($g \propto e^{-z/d}$) in the distal region. In Figure 1a, which highlights the distal region, a straight line with slope $-1/d$ is drawn for comparison; similarly, in the double-logarithmic plot of Figure 1b a line is shown with slope -1 ($\chi = 0$) as predicted by the power law. The volume fraction profile of loops follows from $\varphi^1 = g^2$. As we shall see in section 4.3, plots such as Figure 1 are typical for the plateau region of the adsorption isotherm, where indeed $p \ll d$ for very long chains. (However, in most practical situations the length scales p and d are not well separated.) We define the plateau region as the region where g_1 is of order unity. In the Henry region of the isotherm, where $g_1 \ll 1$ and $p \gg d$, $g \propto e^{-z/d}$ is a purely exponential function with a decay length which is only determined by χ_s; the central region is then absent. This Henry region is discussed in more detail in section 4.3.1.

From eq 32 the extrapolation length $-[\mathrm{d}z/\mathrm{d}\ln g]_{z=0}$ is found as $d \tanh(p/d)$. Hence, for a good solvent in the plateau regime (where $\tanh(p/d) = p/d$) the extrapolation length is p, whereas in the Henry regime (where $\tanh(p/d) = 1$) it equals d.

Once g is known, we can use eqs 23 and 24 to find f. Upon carrying out the integrations of eq 24, we obtain g_0, α_2, and α_1 as $2g_0 = (2\lambda/\nu)^{-1/2} d^2(\cosh x - x/\sinh x)$, $\alpha_2 = (2\lambda/\nu)^{1/2} \ln[\coth(x/2)]$, and $2\alpha_1 = (2\lambda/\nu)^{-1/2} d^3[\sinh x - \kappa(x)]$, where x is given by eq 31a. The function $\kappa(x)$ is defined below (eq 34b). The functions $\alpha_1 g$ and $\alpha_2 g_0$ do not diverge for $x = \infty$, and we choose the integration constants such that $f = 0$ at $z = 1$ (i.e., at $x = x_2$). The result may be written as

$$f = \frac{d^2}{\lambda}[\gamma(x) - \gamma_2(x)] \quad \gamma(x) = \frac{S(x)}{2 \sinh x} \quad \gamma_2(x) = \frac{S(x_2)}{2 \sinh x} \tag{33a,b,c}$$

where $S(x)$ is given by

$$S(x) = \frac{1}{2}(\sinh 2x - 2x)\ln\left[\coth\frac{x}{2}\right] + \sinh x - \kappa(x)$$

$$\kappa(x) = \int_0^x \frac{x'\,\mathrm{d}x'}{\sinh x'} \tag{34a,b}$$

Note that $\nu = 1 - 2\chi$ does not enter these functions explicitly (however, ν affects p and d so that x depends on the solvency). The function $\kappa(x)$ is linear in x for small x, and it approaches a limit $c = \kappa(\infty) = 2.467$ at high x; it may be approximated in high accuracy as $\kappa(x) = c \tanh(x/c)$. The function $S(x)$ is zero for $x = 0$, equals $[1 - 4 \ln (x/2)]x^3/6$ at small x, and approaches asymptotically e^x for large x. The universal function $\gamma_g = \gamma(x)$ for a good solvent is sketched in Figure 2a; it has the limiting behaviors $9\gamma_g = x^2(1 - 3 \ln(x/2))$ at small x and $\gamma_g = 1 - (\pi^2/4)e^{-x}$ at high x, which are also indicated in

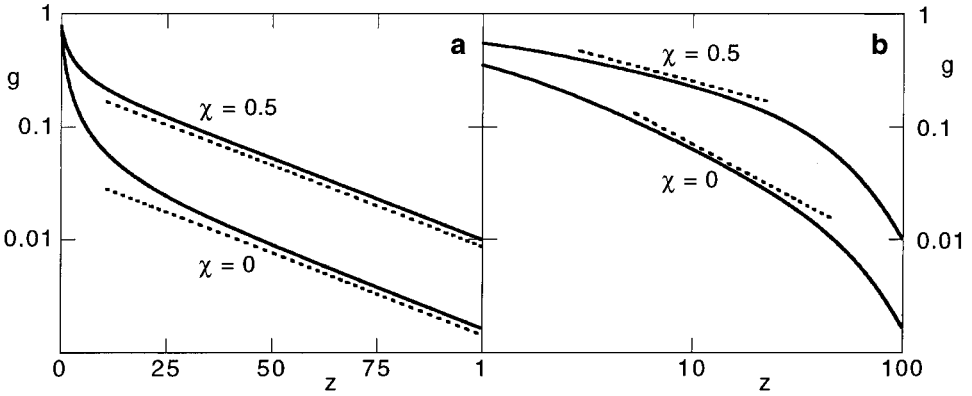

Figure 1. The function $g(z)$ as a function of z in a semilogarithmic (a) and a double-logarithmic plot (b), for $\chi = 0$ (eq 32) and $\chi = 0.5$ (eq 36). In this example the proximal and distal lengths were chosen as $p = 1$ and $d = 30$, and $\lambda = {}^1/_4$. The dotted lines with slope $-1/d$ (a) and -1 and $-{}^1/_2$ (b) are drawn for comparison.

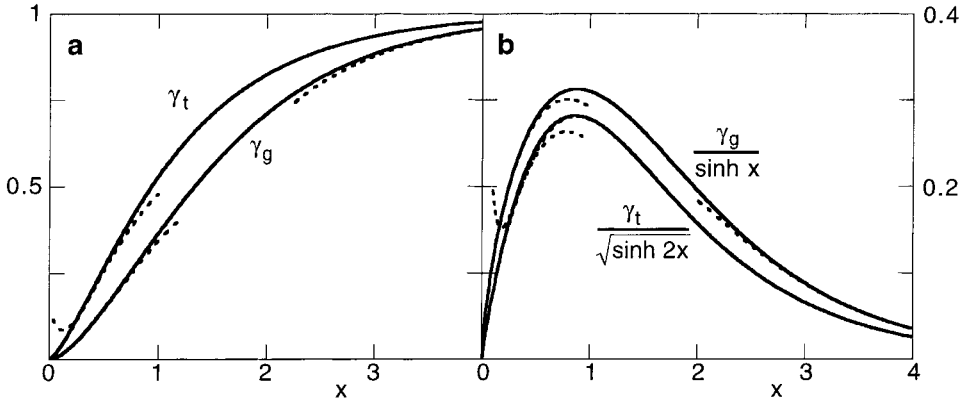

Figure 2. The functions γ_g for good solvents (eq 33b) and γ_t for a Θ solvent (eq 37b) (a) and the normalized tail contributions $\gamma_g/\sinh x$ and $\gamma_t/\sqrt{\sinh 2x}$ (b), drawn as solid curves. The asymptotic expressions for low x ($9\gamma_g = x^2[1 - 3\ln(x/2)]$, eq 39a for γ_t) as well as the limiting expressions for high x ($\gamma_g = 1 - [\pi^2/4]e^{-x}$, eq 39b for γ_t) are given as the dotted curves. Especially eq 39b works extremely well, from high x down to $x \approx 0.2$, below which value the upward curvature shows that this approximation breaks down.

Figure 2a. Under most conditions in the plateau region, the nonuniversal correction γ_2 is small with respect to γ; only in the first few layers its effect is significant. Obviously, for $z = 1$ ($x = x_2$), $\gamma = \gamma_2$.

The tail concentration is proportional to gf (see eq 20), in which the function $\gamma_g/\sinh x$ occurs. This function is sketched in Figure 2b (solid curves), as well as the asymptotes given by the above expressions for γ_g (dotted). The maximum m of the function $\gamma_g/\sinh x$ is $m = 0.3105$ at $x_m = 0.877$; the integral I over this function (from zero to ∞) is $I = 0.733$.

We can now evaluate the integrals I_g, I_{gg}, and I_{gf} defined in eqs 19b and 26. The result is

$$I_g = \sqrt{2\lambda/v}\,\ln[\coth(x_2/2)] \quad I_{gg} = (2\lambda/vd)(\coth x_2 - 1) \tag{35a,b}$$

$$I_{gf} = \frac{2d^2}{\sqrt{2\lambda/v}}\,I(x_2) \quad I(x_2) = \int_{x_2}^{\infty} \frac{\gamma(x) - \gamma_2(x)}{\sinh x}\,\mathrm{d}x \tag{35c,d}$$

The integral $I(x_2)$ is thus smaller than the integral $I = 0.733$ mentioned above; in the plateau region the difference is small. The only other quantities occurring in eqs 27 and 28 are g_1 and g_2, which follow from eq 32 as $g_1 = g(x_1)$ and $g_2 = g(x_3)$. Solving these equations gives p and d as a function of N, χ_s, and φ^b. We discuss the results in section 4.3.

4.2.2. Θ Solvent. The relevant differential equation is eq 17b. The solution is $g = (6\epsilon)^{1/4}\sinh^{-1/2}[2\sqrt{\epsilon/\lambda}(z + p)]$, or

$$g = \frac{(6\lambda)^{1/4}}{\sqrt{d\,\sinh 2x}} \tag{36}$$

which for the plateau regime ($p \ll d$) gives approximately $g \propto z^{-1/2}$ ($\varphi^1 \propto z^{-1}$) in the central region and again $g \propto e^{-z/d}$ in the distal region. The shape of $g(z)$ resembles that in a good solvent (see Figure 1), but the central region is narrower in a Θ solvent; on a double-logarithmic plot (Figure 1b) the slope in this region is now around $-{}^1/_2$.

For a Θ solvent the extrapolation length, equal to $-[\mathrm{d}z/\mathrm{d}\ln g]_{z=0}$, is given by $d\tanh(2p/d)$, according to eq 36. In the plateau regime this is equal to $2p$, whereas in the Henry regime it is again d, like in good solvents.

With eq 36 for g, the functions g_0, α_1, and α_2 can be evaluated from eq 24. Equation 24a gives $2g_0 = (6\lambda)^{-1/4}d^{3/2}(\cosh 2x)/\sqrt{\sinh 2x}$. For the evaluation of α_2 we need the integral $\int \mathrm{d}x/\sqrt{\sinh 2x}$, which can be transformed into an incomplete elliptic integral of the first kind (see, for example, ref 18): $\alpha_2 = (6\lambda)^{1/4}\sqrt{d}[c_1 - F(x)]$, where c_1 is an integration constant and $F(x)$ is defined below (eq 38b).

The function $F(x)$ is sketched in Figure 3. Its limiting behaviors, also given in Figure 3, are $F(x) = \sqrt{2x}$ for

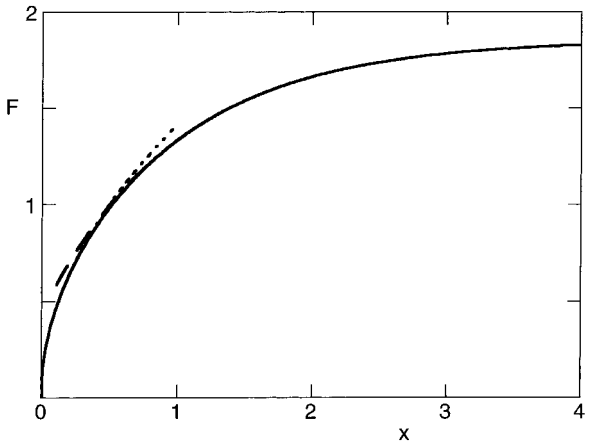

Figure 3. The function $F(x)$ as given by eq 38b (solid curve), and its asymptotic limits $F(x) = \sqrt{2x}$ for small values of x (dotted) and $F(x) = K - \sqrt{2}e^{-x}$ for high values of x (dashed). Here, $K = F(\infty) = 1.854$.

small x and $F(x) = K - \sqrt{2}e^{-x}$ for high x, where $K = F(\infty) = 1.854$ is a complete elliptic integral of the first kind. The integration constant c_1 ensures that $\alpha_2 g_0$ does not diverge exponentially for large x. Hence, $c_1 = K$. The function α_1 is found to be given by $2\alpha_1 = (6\lambda)^{-1/4} d^{5/2} (\sqrt{\sinh 2x} + c_2)$, where c_2 has to be chosen such that $\lambda f = \alpha_1 g + \alpha_2 g_0$ is zero for $x = x_2$. The final result for f can be expressed as

$$f = \frac{d^2}{\lambda}[\gamma(x) - \gamma_2(x)]$$

$$\gamma(x) = \frac{T(x)}{2\sqrt{\sinh 2x}} \quad \gamma_2(x) = \frac{T(x_2)}{2\sqrt{\sinh 2x}} \quad (37a,b,c)$$

where the function $T(x)$ is defined by

$$T(x) = [K - F(x)] \cosh 2x + \sqrt{\sinh 2x} - K$$

$$F(x) = \int_0^{\operatorname{acos}(e^{-x})} \frac{d\psi}{\sqrt{1 - \frac{1}{2}\sin^2\psi}} \quad (38a,b)$$

The function $T(x)$ is zero at $x = 0$, is equal to $x^2[2K - (8/5)\sqrt{2x}]$ at low x, and approaches $\sqrt{2}e^x$ at high x. The function $\gamma_t = \gamma(x)$ for a Θ solvent has approximately the same shape as γ_g for a good solvent, as can be seen in Figure 2a. Using the above limiting expressions for $F(x)$, eq 37b may be expanded in terms of x and e^{-x}, respectively. The result is

$$\gamma_t(x) = x^{3/2}\left(\frac{K}{\sqrt{2}} - \frac{4}{5}\sqrt{x}\right) \quad x \lesssim 0.4 \qquad (39a)$$

$$\gamma_t(x) = 1 - e^{-x}\left(\frac{K}{\sqrt{2}} - \frac{3}{4}e^{-3x}\right)\left(1 + \frac{1}{2}e^{-4x}\right) \quad x \gtrsim 0.4 \qquad (39b)$$

For $x = 0.4$ both expressions give a slightly too low value for $\gamma_t(x)$, but the error is only 2%. These asymptotes are also plotted in Figure 3a. Especially eq 39b is quite accurate over a wide range, down to $x \approx 0.2$.

The function $\gamma_t/\sqrt{\sinh 2x}$, which gives the main contribution to the tail concentration in a Θ solvent, has the same general shape as $\gamma_g/(\sinh x)$ for a good solvent (Figure 2b). In this case the maximum m is $m = 0.281$ at $x_m = 0.862$, and the integral I (from 0 to ∞) equals $I = 0.606$.

The integrals I_g, I_{gg}, and I_{gf} are given by

$$I_g = (6\lambda)^{1/4}\sqrt{d}(K - F(x_2)) \quad I_{gg} = \sqrt{3\lambda/2}\,\ln(\coth x_2) \qquad (40a,b)$$

$$I_{gf} = \frac{(6\lambda)^{1/4} d^{5/2}}{\lambda} I(x_2) \quad I(x_2) = \int_{x_2}^{\infty} \frac{\gamma(x) - \gamma_2(x)}{\sqrt{\sinh(2x)}}\,dx \qquad (40c,d)$$

and g_1 and g_2 in eqs 27 and 28 are again $g_1 = g(x_1)$ and $g_2 = g(x_3)$.

4.3. Asymptotic Expressions for *p* and *d*. Generally, the parameters p and d ($=\sqrt{\lambda/\epsilon}$) have to be found numerically from eqs 27 and 28 in combination with eqs 32 and 35 (good solvents) or eqs 36 and 40 (Θ solvent). An example for $\chi = 0$ is shown in Figure 4. A similar plot for $\chi = 0.5$ looks nearly the same, with only minor quantitative differences, so that in Figure 4 we restrict ourselves to $\chi = 0$. Figure 4a gives p and d^2 as a function of N for $\chi_s = 1$ and $\varphi^b = 10^{-25}$, Figure 4b gives p and $1/d^2$ as a function of $\log(1/\varphi^b) = 0.43y^2$ for $\chi_s = 1$ and $N = 100$, and Figure 4c shows the dependence of p and d on χ_s for fixed N (=100) and φ^b (=10^{-25}). The numerical solution is shown as the solid curves.

The parameter set ($N = 100$, $\chi_s = 1$, and $\varphi^b = 10^{-25}$) was chosen such that the transition from the Henry region (low N, low φ^b, low χ_s) to the plateau regime (higher N, φ^b, χ_s) is clearly visible. In the Henry region, p decreases linearly with increasing N (Figure 4a), increases linearly with increasing y^2 (Figure 4b), and decreases with increasing χ_s (Figure 4c). In the same regime, d does not depend on N (Figure 4a) or y (Figure 4b), and it decreases with increasing χ_s, though less strongly than p (Figure 4c). In the plateau regime, p is nearly independent of N (Figure 4a) and y (Figure 4b), and it decreases gradually with increasing χ_s (Figure 4c). In this regime d increases proportionally with $\sqrt{N}$ (Figure 4a), it is inversely proportional to y (Figure 4b), and it decreases slightly with increasing χ_s (Figure 4c).

These trends may be interpreted by considering limiting expressions for g_1, g_2, I_g, and I_{gg} at large x (Henry region) and at small x (plateau region), respectively. In these asymptotic expressions the term I_{gf} in eq 27 will be neglected.

4.3.1. Henry Region. In the Henry regime the dilute surface layer is composed of individual adsorbed chains in equilibrium with the (extremely) dilute solution. When χ_s is very close to the critical adsorption energy χ_{sc}, which is the adsorption threshold for infinitely long chains, the adsorbed chains form dilute coils with relatively few surface contacts, and they are only weakly perturbed from a random coil. At higher χ_s the chains flatten and form a so-called pancake, with a higher fraction of the segments in contact with the surface. Equality of the chemical potentials in bulk and at the surface demands that $\Gamma \propto \varphi^b e^{N\epsilon}$, where $N\epsilon$ is the free energy gain for an adsorbed chain. The relation between ϵ and $\Delta\chi_s \equiv \chi_s - \chi_{sc}$ can be found from scaling arguments.[19] In the following we keep Gaussian statistics for consistency with the mean-field approach.

At critical adsorption ($\chi_s \approx \chi_{sc}$), coils with a finite number of segments do not flatten and have only about $\sqrt{N}$ contacts with the wall (as found from Gaussian statistics). The free energy gain per chain in this weak

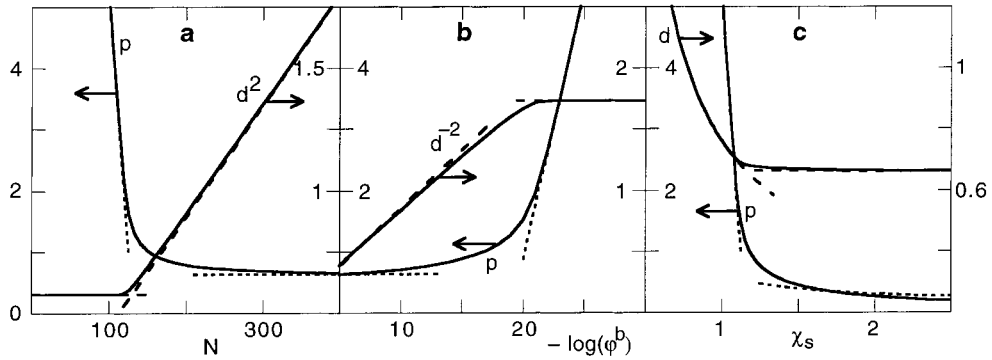

Figure 4. The length scales p and d in a good solvent ($\chi = 0$) as a function of N (at $\chi_s = 1$ and $\varphi^b = 10^{-25}$) (Figure 4a), as a function of $\log(1/\varphi^b)$ (for $\chi_s = 1$ and $N = 100$) (Figure 4b), and as a function of χ_s (for $N = 100$ and $\varphi^b = 10^{-25}$) (Figure 4c). The solid curves were obtained by solving eqs 27 and 28. The dotted curves are asymptotic expressions for p in the Henry region (eq 43) and in the plateau region (eq 45a), the dashed curves are asymptotes for d (eq 41a and 46, respectively). In these diagrams, the left-hand scales apply to p, and the right-hand scales to d^2 (Figure 4a), d^{-2} (Figure 4b), and d (Figure 4c), respectively.

adsorption regime is $\sqrt{N}\Delta\chi_s$. This gain should be unity (1 kT) at the adsorption threshold. At slightly higher χ_s the chain flattens ($\sqrt{N}\Delta\chi_s > 1$), and we enter the strong adsorption regime. We can then subdivide the chain in blobs of g units ($g \ll N$), such that $\sqrt{g}\Delta\chi_s = 1$; these blobs are still Gaussian and are isotropic subunits of the chain. The free energy gain per monomer is $1/g$ (in units of kT), so that $\epsilon \approx 1/g \propto (\Delta\chi_s)^2$ in this regime. We denote this situation as a fluffy pancake.

At still higher χ_s the pancake thickness reduces to the monomer size and $g \approx 1$ ($g < 1$ is meaningless): about every monomer touches the wall, and we have flat pancakes. For those high surface affinities $\epsilon \propto \Delta\chi_s$. The crossover between the fluffy pancake regime and the regime of very strong adsorption (flat pancakes) is expected around $\Delta\chi_s \approx (\Delta\chi_s)^2 \approx 1$. At this value of χ_s, we are still in the Henry regime if $\Gamma = \varphi^b e^N$ is small, hence if $y^2 = \ln(1/\varphi^b) \gg N$. The crossover toward the plateau regime occurs when y^2 is of order (but below) N. A more precise formulation of this latter crossover (also for other values of χ_s) is given in eq 44.

Strictly speaking, our mean-field approach, based upon average concentrations parallel to the wall, is not valid for individual coils or pancakes. Nevertheless, we will see that our treatment, though a priori inaccurate, correctly reproduces the two types of behavior discussed above. Moreover, it gives access to the growth of the layer at and just beyond the crossover to the plateau regime, where information is lacking so far.

We may approximate eq 28b in the Henry regime as $u_1 = -\chi_s - \lambda\chi$ since g_1^2 and g_2^2 in this regime are very small. Moreover, $p \gg d$ in this regime (see Figure 4), which makes that the terms "proximal length" for p and "distal length" for d are no longer suitable. The term exponential decay length or cutoff length for d is still appropriate; d becomes now also the extrapolation length and is the only length scale. The parameter p loses its meaning and does not enter the equations.

Because $p \gg d$, $\sinh x_1$ may be replaced by $e^{x_1}/2$. Then $g_2/g_1 = e^{-1/d}$ does not depend on p, and the parameter d can be computed from eq 28, which is simplified to

$$\frac{\lambda}{d_h^2} = \chi_s + \lambda\chi + \ln(\lambda_0 + \lambda e^{-1/d_h}) = \Delta\chi_s + \ln\left[1 - \frac{\lambda}{1-\lambda}(1 - e^{-1/d_h})\right] \quad (41a)$$

where we used the subscript h to denote the Henry region. The parameter $\Delta\chi_s$ is defined as $\chi_s - \chi_{sc}$, with $\chi_{sc} = -\ln(1-\lambda) - \lambda\chi$. The first term (which is the only one for $\chi = 0$) has an entropic origin; the second one is an energetic contribution caused by the fact that when $\chi > 0$ an adsorbed segment loses a fraction λ of its unfavorable contacts with the solvent. For a monomeric adsorbate, where the entropic contribution is absent, this energetic part leads to some adsorption even when χ_s is zero.

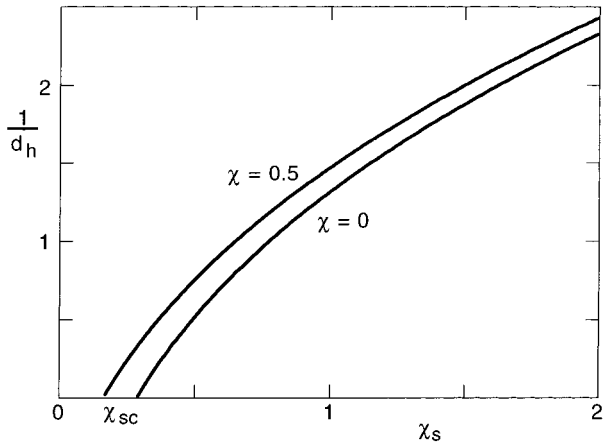

Figure 5. The exponential decay length d_h in the Henry region as a function of χ_s, for $\lambda = 1/4$. The curves were computed from the implicit eq 41a, but the explicit eq 41b gives virtually identical results (the numerical differences are less than 0.1%). The two curves for $\chi = 0$ and $\chi = 0.5$ are shifted by an amount $\lambda\chi = 0.125$ along the abscissa axis. Results for intermediate solvencies are found by interpolating according to $\lambda\chi$.

According to eq 41a, the extrapolation length d_h depends only on the parameter combination $\chi_s + \lambda\chi$. Note that in the plateau regime, to be discussed in the next section, the extrapolation length is also coupled to $\chi_s + \lambda\chi$; however, this length is then related to p. The numerical solution of eq 41a is shown in Figure 5. This solution is also given in the three diagrams of Figure 4 (dashed curves). For $\lambda = 1/4$, $\chi_s = 1$, and $\chi = 0$, $d_h = 0.760$ so that the asymptotes in Figures 4a (for low N) and 4b (for low φ^b) are horizontal lines.

Equation 41a constitutes an implicit equation in d_h. While preparing this paper, we learned that Gorbunov and Skvortsov[20] obtained, along quite different lines, an explicit expression for the extrapolation length for $\chi = 0$, which they defined through $1/d_h = -[\mathrm{d} \ln G/\mathrm{d}z]_{z=0}$, where G is the end-point distribution of a single adsorbing end-attached chain. For such a chain, Rubin[21]

derived analytically the partition function in a lattice model. Using this result, Gorbunov and Skvortsov arrived at

$$\frac{\lambda}{d_h^2} = \ln m - \ln\left[1 - \frac{1}{2\lambda}\left(1 - \sqrt{1 + 4\lambda(m-1)}\right)\right]$$

$$m = \frac{\lambda}{1 - e^{-\chi_{sc}}} = \frac{1 - e^{-\chi_{sc}}}{1 - e^{-\chi_s}} \quad (41b)$$

On the left-hand side, we replaced $1/(6d_h^2)$ in the original equation (where d_h is expressed in units of the bond length) by λ/d_h^2 so that d_h is now in units of lattice spacing, as in eq 41a. The parameter m in eq 41b runs from 1 at the critical point to λ at very high χ_s.

Although eqs 41a and 41b are mathemathically not equivalent, they give numerically virtually identical results, with a maximum deviation of less than 0.1%. We intend to discuss this surprising result in a forthcoming publication.

Both equations give the same limit for χ_s close to χ_{sc}: $1/d_h = (1/\lambda - 1)\Delta\chi_s$. This may be compared with the scaling results. Since the free energy per segment (in units of kT) equals $\epsilon = \lambda/d_h^2$, we have $\epsilon = \lambda^{-1}(1 - \lambda)^2 \Delta\chi_s^2$, in this regime, in full agreement with scaling. Our GSA description applies in the strong adsorption regime $\sqrt{N}\Delta\chi_s > 1$. Usually one introduces a crossover exponent ϕ, such that $N^\phi\Delta\chi_s \approx 1$ defines the crossover line from weak to strong adsorption; in our case the exponent ϕ takes its mean-field value $^1/_2$. In terms of d_h, the condition $\sqrt{N}\Delta\chi_s > 1$ may also be written as $d_h \lesssim \lambda\sqrt{N}$.

At high χ_s the reciprocal length $1/d_h$ is proportional to $\sqrt{\chi_s}$: both equations predict for this limit $\lambda/d_h^2 = \chi_s + \lambda\chi + \ln\lambda_0$, which may be identified with the segmental free energy ϵ. Again this agrees with the scaling prediction.

We can now find the value of b and g_1 in the Henry region from substituting d_h into eq 27. With $\sinh x = e^x/2$, $\coth x = 1 + 2e^{-2x}$, $\ln\coth x/2 = 2e^{-x}$, and $K - F(x) = \sqrt{2}e^{-x}$, we derive easily that $I_{gg} = (d_h/2)e^{-1/d_h}g_1^2$ and $I_g = d_h e^{-1/(2d_h)}g_1$ for both good solvents and for a Θ solvent. Neglecting the term I_{gf} in eq 27b (which is allowed in the strong adsorption regime because the contribution of tails is then small), we find $g_1 = A_h b$, where A_h is a constant of order unity. Since $b^2 = \exp(-y^2 + \lambda N/d_h^2) = \varphi^b e^{\lambda N/d_h^2}$, we may write

$$g_1^2 = A_h^2\,\varphi^b e^{\lambda N/d_h^2} \quad A_h = \frac{1 + d_h e^{-1/(2d_h)}}{1 + (d_h/2)e^{-1/d_h}} \quad (42a,b)$$

which may be considered as the adsorption isotherm equation in the Henry region. (The total adsorbed amount Γ equals $g_1^2 + I_{gg}$, so that for Γ the prefactor in eq 42a is just the square of the numerator of A_h.) Hence, we find $\ln(\Gamma/\varphi^b) \propto N/d_h^2$, which gives $\ln(\Gamma/\varphi^b) \propto N(\Delta\chi_s)^2$ at low χ_s (fluffy pancakes) and $\ln(\Gamma/\varphi^b) \propto N\chi_s$ at higher χ_s (flat pancakes), just as in the mean-field scaling description presented in the introduction of this section.

The equations derived so far in this section are valid for both good solvents and for a Θ solvent. We may also calculate p_h, even though this parameter is not really important in the Henry regime. Now a small difference shows up for different solvencies because v enters the prefactor in g. We write $g_1^2 = B_h^2\, e^{-(2p_h+1)/d_h}$, where $B_h^2 = (8\lambda/v)d_h^2$ for good solvents and $B_h^2 = 2\sqrt{6\lambda}/d_h$ for $\chi = 0.5$. Upon identification of this expression for g_1^2 with eq 42a, we find for p_h:

$$p_h = \frac{d_h}{2}\left(y^2 - \frac{\lambda N}{d_h^2}\right) + d_h \ln\frac{B_h}{A_h} - \frac{1}{2} \quad (43)$$

The last two terms constitute only a small correction. The asymptotic dependence according to eq 43 is plotted in the three diagrams of Figure 4 for $\chi = 0$ (dotted curves for small N, small φ^b, and small χ_s, respectively) and agrees very well with the numerical solution of the two simultaneous eqs 27 and 28 in the Henry regime.

In the next section, we derive expressions for d_p and p_p in the plateau regime. We will see that p_p depends only on χ_s and is of order unity (or below) unless $\Delta\chi_s$ is very small. We can localize the crossover between the Henry and plateau regimes by demanding $p_p = p_h$ or $d_p = d_h$. Both criteria give essentially the same result. We choose $p_p = p_h$ because in this way we do not need the value of b (see eq 47 below; at the crossover point b equals $b(p_p,d_h)$ and is only a function of χ_s). Omitting the small correction terms in eq 43, we find for the crossover point:

$$y^2 - \frac{\lambda N}{d_h^2} = \frac{2p_p}{d_h} \quad (44)$$

Since in most cases $p_p \ll \lambda N/d_h$, eq 44 basically reads $d_0 = d_h$, where $d_0 = \sqrt{\lambda N}/y$ depends only on N and φ^b, and d_h is only a function of χ_s. For $\chi_s = 1$ and $\lambda = {}^1/_4$, as in Figure 4a,b, $d_h = 0.76$ (eq 41). We will see below (Figure 6) that $p_p = 0.595$ for $\chi = 0$ under those conditions. Then eq 44 predicts a crossover at $N = 129$ in Figure 4a and at $\log(\varphi^b) = -19.5$ in Figure 4b, which does indeed correspond with the intersection point of the two asymptotes. In Figure 4c the crossover point

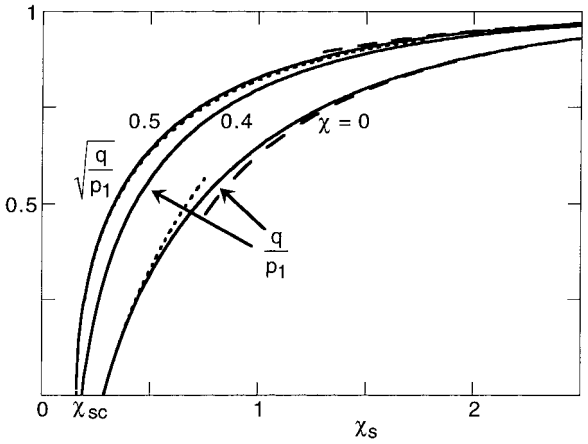

Figure 6. The proximal length $p_p = p_1 - {}^1/_2$ as a function of χ_s in the plateau region, plotted as q/p_1 ($= \sqrt{\varphi_1}$) for two good solvents ($\chi = 0$ and 0.4), and as $\sqrt{q/p_1}$ ($= \sqrt{\varphi_1}$) for a Θ solvent, for $\lambda = {}^1/_4$. Here, $q = (2\lambda/v)^{1/2}$ for a good solvent and $q = (6\lambda/4)^{1/2}$ for a Θ solvent. Solid curves correspond to the solution of eqs 45a and 47a. The asymptotic relations for $\chi = 0$ and $\chi = 0.5$ at small $\chi_s - \chi_{sc}$ (eqs 45b and 47b, dotted) and at high χ_s (eqs 45c and 47c, dashed) are also indicated. The critical adsorption energy χ_{sc} equals $-\ln(1 - \lambda) - \lambda\chi$, which gives 0.288, 0.188, and 0.163, respectively, for $\chi = 0$, 0.4, and 0.5. The proximal length p_p diverges for $\chi_s \to \chi_{sc}$, and at high χ_s it reaches a constant level $p_\infty = 0.207$, 1.081, and 0.112 for $\chi = 0$, 0.4, and 0.5.

has to be calculated by solving (for given y and N) the implicit eq 44 for χ_s (both p_p and d_h depend on χ_s); the result for $N = 100$ and $\varphi^b = 10^{-25}$ is $\chi_s = 1.15$.

4.3.2. Plateau Region in Good Solvents. Next we turn our attention to the plateau regime. For this regime, we use the subscript p. Now we assume $d_p \gg p_p$ so that $\sinh x_1 = x_1$. (For the example of Figure 4, with relatively short chain lengths, this condition is not fully satisfied, as d_p is only slightly above p_p. Nevertheless, we will see that even in this case the asymptotic relations for the plateau region, to be derived below, work reasonably well.) A further approximation is that in eq 28 ϵ, which is now small with respect to u_1, may be omitted. Under these conditions d_p drops out of eq 28, so that this equation may be solved for p_p as the only unknown parameter.

In the plateau region we have $g_1 = q/p_1$, $g_2 = q/p_3 = q/(p_1 + 1)$, and $g_2/g_1 = 1/(1 + 1/p_1)$, where $p_1 = p_p + {}^1/_2$ (eq 31c); it turns out that the equations for p_p are most easily formulated in terms of p_1. The parameter $q \equiv (2\lambda/v)^{1/2}$ equals $p_\infty + {}^1/_2$, where p_∞ is the proximal length for $\chi_s \rightarrow \infty$. Equation 28 for good solvents gives now

$$e^{-\chi_s-\lambda\chi} = \left(1 - \frac{q^2}{{p_1}^2}\right)\left(\lambda_0 + \frac{\lambda}{1 + 1/p_1}\right) \times \exp\left[2\chi\frac{q^2}{{p_1}^2}\left(\lambda_0 + \frac{\lambda}{(1 + 1/p_1)^2}\right)\right] \qquad q \equiv p_\infty + \frac{1}{2} = \sqrt{\frac{2\lambda}{1 - 2\chi}} \quad (45a)$$

Note that the term $1 - {g_1}^2$, which was set unity in the Henry region, is now important since $\varphi_1 = {g_1}^2$ may be high. Equation 45a constitutes an implicit equation in p_1 which can be solved numerically. The solution for p_1 as a function of χ_s for $\lambda = {}^1/_4$ is given in Figure 6, for two good solvents, $\chi = 0$ (lower solid curve) and $\chi = 0.4$ (middle solid curve). We plot the ratio q/p_1, which for good solvents is equal to the square root of the train density φ_1. For χ_s close to χ_{sc}, q/p_1 is small so that the proximal length p_p is large. For higher χ_s, q/p_1 increases (p_p decreases) until at high χ_s a level $q/p_{1,\infty} = 1$ is reached. Note, however, that q is not the same in both solvencies. Since q is inversely proportional to $\sqrt{v}$, p_1 increases with increasing χ roughly as $\sqrt{1/v}$ (except close to χ_{sc}). As a consequence, the plateau approximation breaks down for small v (χ close to 0.5) because the condition $p \ll d$ is no longer satisfied.

From the implicit eq 45a, explicit approximations for small $\Delta\chi_s$ and for high χ_s may be derived. For small $\Delta\chi_s$ the first factor (which is $1 - \varphi_1$) in eq 45a is close to unity. The second factor is then approximately equal to $e^{-\chi_{sc}-\lambda\chi} = 1 - \lambda$. Expanding the right-hand side of eq 45a up to second order in $1/p_1$, we obtain a quadratic equation in $1/p_1$. Its solution may be written as

$$\frac{q}{p_1} = \frac{q}{2B}\left(\sqrt{1 + \frac{4B}{\lambda}e^{-\lambda\chi}(e^{-\chi_{sc}} - e^{-\chi_s})} - 1\right) \qquad B = (1 - \lambda)(q^2 - 2\lambda + 2) - 1 \quad (45b)$$

For the special case $\chi = 0$, where $q^2 = 2\lambda$, the function B equals λ_0. The dependence of q/p_1 on χ_s according to this equation is given in Figure 6 as the dotted curve for $\chi = 0$; it is accurate only for $\Delta\chi_s < 0.2$. The limiting behavior of eq 45b is $1/p_1 = e^{-\lambda\chi}(e^{-\chi_{sc}} - e^{-\chi_s})/\lambda$, which for even smaller $\Delta\chi_s$ reduces to $p_1 \approx \lambda e^{\lambda\chi}/\Delta\chi_s$. The scaling dependence $p_p \propto {\Delta\chi_s}^{-1}$ has been derived before.[17]

For high χ_s the factor $1 - \varphi_1 = 1 - q^2/{p_1}^2$ in eq 45a is small and the most important one. An approximate expression for p_1 in this case follows from substituting $p_{1,\infty} = q$ into the second factor:

$$\frac{q^2}{{p_1}^2} = 1 - s_1 e^{-\chi_s-\chi(\lambda+2/s_2)} \qquad \frac{1}{s_i} = \lambda_0 + \frac{\lambda}{(1 + 1/q)^i}$$

$$p_1\left(\chi = 0, \lambda = \frac{1}{4}\right) = \frac{1}{\sqrt{2(1 - 1.66e^{-\chi_s})}} \quad (45c)$$

This approximation leads to the dashed curve in Figure 6 for $\chi = 0$; it is reasonably accurate above $\chi_s = 1$.

With the proximal length p_p known from eq 45, we may use eq 27 to find the distal length d_p. It turns out that the term $\ln b$ is now a small correction and d_p is close to (but higher than) d_0. In principle, d_p should be calculated by solving the implicit eq 27a with $b = b(p_p,d_p)$ for d_p. A rather accurate explicit approximation is obtained by inserting p_p and d_0 into the correction term, omitting again the term I_{gf}. Hence

$${d_p}^2 = \frac{\lambda N}{y^2 + 2\ln b_0} \qquad b_0 = g_1\frac{1 + d_0\sinh^2 x_1\,(\coth x_2 - 1)}{1 + d_0\sinh x_1\ln[\coth(x_2/2)]} \qquad g_1 = \frac{\sqrt{2\lambda/v}}{d_0\sinh x_1} \quad (46a,b,c)$$

where $x_1 = (p_p + {}^1/_2)/d_0$ and $x_2 = (p_p + 1)/d_0$. We avoid the approximations $\sinh x = x$ and $\coth x = 1/x$ in eq 46b in order to make this equation more suitable for short chains (as in Figure 4).

The asymptotic relations 45a and 46a work quite reasonably in the plateau region, even for relatively short chains, as indicated in Figure 4. In Figure 4a,b, where χ_s is constant, $p_p = 0.595$, and in Figure 4c p_p slowly decreases with increasing χ_s, approaching the value $1/\sqrt{2} - {}^1/_2 = 0.207$ for very high χ_s. Equation 46 describes d_p quite well, as seen in Figure 4 (dashed curves for high N, high φ^b, and high χ_s, respectively). The (weak) decrease with χ_s in the plateau region of Figure 4c is due to the correction term b_0. For very high χ_s, d_p approaches $d_0 = \sqrt{\lambda N}/y = 0.66$ (Figure 4c).

4.3.3. Plateau Region in a Θ Solvent. As for a good solvent, we assume $\sinh x = x$ and $\epsilon \ll u_1$. The proximal length $p_p = p_1 - {}^1/_2$ then follows from eq 28 with $\chi = 0.5$:

$$e^{-\chi_s-\lambda/2} = \left(1 - \frac{q}{p_1}\right)\left(\lambda_0 + \frac{\lambda}{\sqrt{1 + 1/p_1}}\right) \times \exp\left[\frac{q}{p_1}\left(\lambda_0 + \frac{\lambda}{1 + 1/p_1}\right)\right] \qquad q \equiv p_\infty + \frac{1}{2} = \frac{\sqrt{6\lambda}}{2} \quad (47a)$$

which may be numerically solved for p_1; the solution in the form $\sqrt{q/p_1}$ as a function of χ_s is plotted in Figure 6. For a Θ solvent q/p_1 equals the train density φ_1. In the same way as for eq 45 limiting expressions for χ_s close to χ_{sc} and for high χ_s may be derived. At $\chi_s = \chi_{sc} = -\ln(1 - \lambda) - \lambda/2$ we have again $1/p_1 = 0$.

In the weak adsorption limit we expand the right-hand side of eq 47a up to second order in $1/p_1$ to obtain

again a quadratic equation in $1/p_1$. The solution is slightly more complicated than eq 45b for a good solvent:

$$\frac{q}{p_1} = \frac{qA}{2B}\left(\sqrt{1 + \frac{4B}{\lambda A^2}e^{-\lambda/2}(e^{-\chi_{sc}} - e^{-\chi_s})} - 1\right)$$

$$B = q\left(1 - \frac{3}{2}\lambda\right) + \frac{3}{4}(\lambda_0 - 2\lambda^2 + 2\lambda^3) \quad (47b)$$

where now $q^2 = 3\lambda/2$ and where the constant $A \equiv q(1 - \lambda) + {}^1/_2$ is close to unity. For small $\Delta\chi_s$, $1/p_1$ approaches $e^{-\lambda/2}(e^{-\chi_{sc}} - e^{-\chi_s})/\lambda A \approx \Delta\chi_s/(\lambda e^{\lambda/2})$, which is nearly the same result as for good solvents.

For high χ_s ($\varphi_1 \approx 1$), p_1 is again found by substituting $p_1 = q$ into eq 47a (except in the first factor):

$$\frac{q}{p_1} = 1 - s_{0.5}e^{-\chi_s - \lambda/2 - 1/s_1} \quad p_1\left(\lambda = \frac{1}{4}\right) = \frac{0.612}{1 - 0.744e^{-\chi_s}} \quad (47c)$$

where the s functions are defined in eq 45c (with $q^2 = 3\lambda/2$). The dependence of $\sqrt{q/p_1}$ ($=\sqrt{\varphi_1}$) on χ_s for $\chi = 0.5$ according to the limiting expressions 47b and 47c is also given in Figure 6.

Once p_p is known, d_p can be calculated in the same way as for good solvents. Analogously to eq 46 we have

$$d_p{}^2 = \frac{\lambda N}{y^2 + 2\ln b_0}$$

$$b_0 = g_1 \frac{1 + 0.5d_0 \sinh 2x_1 \ln[\coth x_2]}{1 + d_0\sqrt{\sinh 2x_1}(K - \sqrt{2x_2})}$$

$$g_1 = \frac{(6\lambda)^{1/4}}{\sqrt{d_0 \sinh 2x_1}} \quad (48a,b,c)$$

where again $x_1 = (p_p + {}^1/_2)/d_0$ and $x_2 = (p_p + 1)/d_0$.

5. Comparison of Analytical and Numerical Results

In this section, we give a few illustrative examples of analytical results obtained with the equations derived in section 4, and we compare them with the numerical SCF computations according to the lattice model as described in section 2. In most cases, we will only consider the extremes $\chi = 0$ and $\chi = 0.5$; however, in Figure 16 we discuss also intermediate solvencies. We start by checking a number of assumptions made in the analytical derivations.

5.1. Check of the GSA Assumptions on the Numerical Results. The central assumption in the GSA formalism is eq 14, which presupposes that each segment in the chain would contribute a constant factor e^{ϵ} to the end-point distribution $G^a_{z,s}$ of adsorbed chains. Since $G^a_{z,s}$ is computed in high accuracy in the numerical model, we can calculate the ratio $R_{z,s} = G^a_{z,s+1}/G^a_{z,s}$ and plot this ratio as a function of s for several layers. Figure 7 gives an example for $N = 10^3$, $\chi_s = 1$, $\varphi^b = 10^{-6}$, and $\chi = 0$. In the first layer, $R_{1,s}$ decreases steeply from a value around 1.04 for $s = 1$ to a final value 1.0116 for s around 100; for all the remaining 900 segments the same value for $R_{1,s}$ applies. It is easily understood why $R_{z,s}$ deviates for small s. For example, $R_{1,1}$ in the numerical model equals $G_1(\lambda_0 + \lambda G_2/G_1)$ according to eq 2; here $G_z = e^{-u_z}$ as defined in eq 3b. In the GSA approach, $R_{1,s}$ is given by e^{ϵ} for any s, which can be written as $G_1(\lambda_0 + \lambda g_2/g_1)$ on account of the boundary

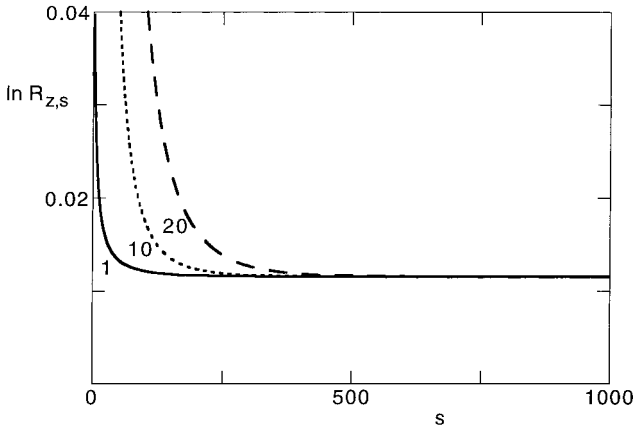

Figure 7. The ratio $R_{z,s}$, defined as $G^a_{z,s+1}/G^a_{z,s}$, as a function of s for three layers: $z = 1$, 10, and 20. The data were obtained from the numerical SCF model with $\lambda = {}^1/_4$, $N = 10^3$, $\chi_s = 1$, $\varphi^b = 10^{-6}$, and $\chi = 0$.

constraint 28a. Under the given conditions, G_2/G_1 is larger than $g_2/g_1 \approx p_1/p_3$, so that the numerical result for $R_{1,1}$ is larger than e^{ϵ}. Nevertheless, the GSA result is quite accurate for most of the chain segments. The same applies for other layers; in Figure 7 results are also given for $z = 10$ and $z = 20$. The same final level is reached, but the deviations at small s are larger. This is to be expected because in the exact model $G^a_{z,s} = 0$ for $s < z$, so that the GSA assumption $R_{z,s} = e^{\epsilon}$ breaks down completely for $s < z$.

For high s in Figure 7 the numerical value for ϵ is 0.011 56, which corresponds to $d = 1/\sqrt{4\epsilon} = 4.650$. The solution of eqs 27 and 28 gives $d = 4.624$, which is quite close. In this case the asymptotic limit for the plateau region works also quite well: with $p = 0.595$ (eq 45a), eq 47 gives $d = 4.633$.

Hence, the numerical SCF results can be used to extract the distal length d from $R_{z,s}$ for large s. Once d is known, a numerical value for p may be found from $g_1 = \sqrt{\varphi_1}$; for $\chi = 0$ we have $p = d\ \mathrm{asinh}\sqrt{2\lambda/\varphi_1 d^2} - {}^1/_2 \approx \sqrt{2\lambda/\varphi_1} - {}^1/_2$. For the example of Figure 7 the train density φ_1 equals 0.3938, which gives $p = 0.616$. This value may be compared with the value $p = 0.598$ obtained from eqs 27 and 28 and with the asymptotic value 0.595 used above; again the agreement is quite good. In this way, the parameters p and d can be computed from the numerical SCF results for a wide range of conditions (e.g., such as given in Figure 4). Then a similar plot as Figure 4 may be constructed, based upon the "numerical" values derived from the SCF data. The difference with the actual Figure 4 (where eqs 27 and 28 were used to obtain p and d) is hardly visible, so that we do not give this plot. We conclude that eqs 27 and 28 (and their asymptotic versions for the Henry and plateau regimes) give an accurate estimate for the proximal and distal lengths.

A second important step in the analytical model is the relation between u and φ, which for $z > 1$ was taken as $u = \varphi$ ($\chi = 0$) or $u = \varphi^2/2$ ($\chi = 0.5$). Figure 8 gives a numerical SCF example to check these dependencies. Figure 8a gives u ($= -\ln G$) and φ ($= \varphi^l + \varphi^t + \varphi^f$) as obtained from the numerical results for $\chi = 0$. It is clear that the agreement between u and φ is quite good. Only in the periphery of the adsorbed layer, where φ approaches φ^b, does the expected deviation occur because here the value of φ^b is no longer negligible (here $u = \varphi$

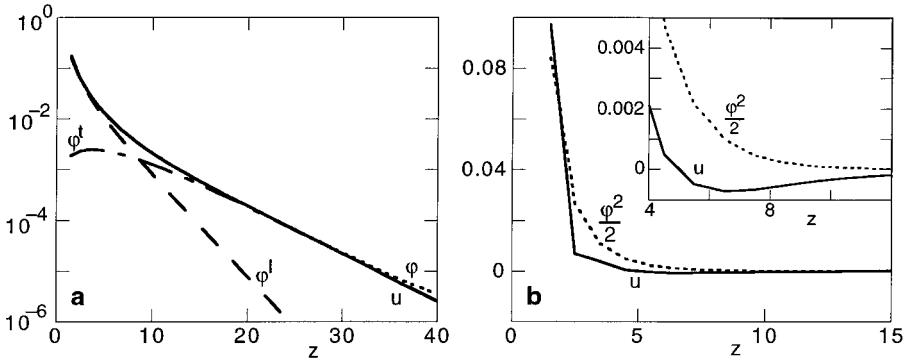

Figure 8. Comparison of u with φ for $\chi = 0$ (left) and of u with $\varphi^2/2$ for $\chi = 0.5$ (right). All data were taken from numerical SCF computations for $N = 10^3$, $\varphi^b = 10^{-6}$, $\chi_s = 1$, and $\lambda = {}^1/_4$. For the good solvent, u and φ are plotted on a logarithmic scale; for comparison the loop and tail contributions to φ are also indicated. For the Θ solvent u is negative over several layers so that a linear scale was used; the inset shows more details for layers 4−10.

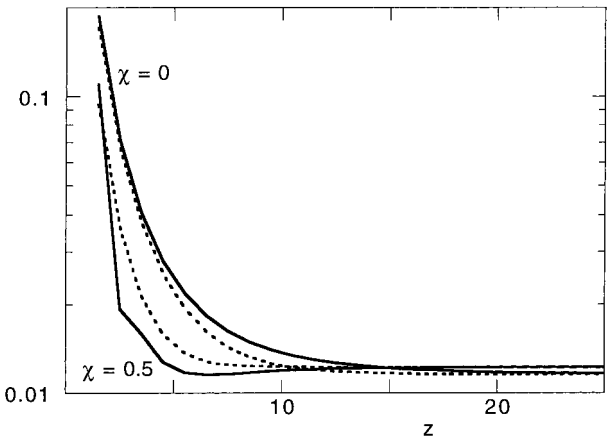

Figure 9. Comparison of $\epsilon + u$ with $\epsilon + \varphi^l$ for $\chi = 0$ (top curves) and of $\epsilon + u$ with $\epsilon + (\varphi^l)^2/2$ for $\chi = 0.5$ (bottom curves). The solid curves are $\epsilon + u$, the dotted curves $\epsilon + \varphi^l$ ($\chi = 0$) or $\epsilon + (\varphi^l)^2/2$ ($\chi = 0.5$). All data are numerical SCF results, for the same conditions as in Figure 8.

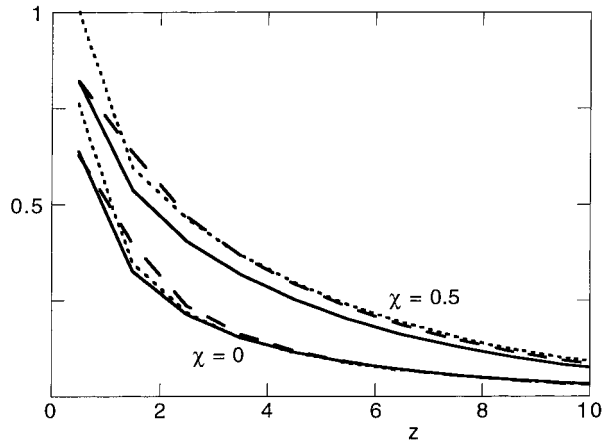

Figure 10. Comparison of the ground-state eigenfunction g (solid curves) with $(\varphi^{trl})^{1/2} \equiv (\varphi^{tr} + \varphi^l)^{1/2}$ (dashed) and $(N/2b)\varphi^{ae}$ (dotted) for $\chi = 0$ (bottom curves) and $\chi = 0.5$ (top curves). The function g is the analytical expression, and φ^{tr}, φ^l, and φ^{ae} are numerical SCF results. Conditions: $N = 10^3$, $\varphi^b = 10^{-6}$, $\chi_s = 1$, and $\lambda = {}^1/_4$.

$- \varphi^b$ applies). It can also be seen in Figure 8a that $u = \varphi^l$ is only accurate in the inner region of the adsorbed layer. In the outer region, $u = \varphi^t$ would be a much better approximation.

In the differential eq 15 the approximation was made to replace $\epsilon + u$ by $\epsilon + \varphi^l$ for $\chi = 0$. According to Figure 9 (top curves), this is a reasonable approximation: in the region just beyond the maximum in φ^t, $\epsilon + \varphi^l$ is lower than $\epsilon + u$, as expected, but the difference is (in this example) never more than about 15%. Consequently, this approximation works reasonably well in a good solvent.

For a Θ solvent, the approximation $u = \varphi^2/2$ is less accurate, as seen in Figure 8b. As a matter of fact, u in this case becomes negative over several layers, which makes a logarithmic plot (as given in Figure 8a) impossible. The reason for the negative u values is that nonlocal energy effects in eq 4 become important in a Θ solvent. In GSA, eq 13 for $\chi = 0.5$ is approximated as $u = \varphi^2/2$, but if the last term of eq 13 is included, we have $u = \varphi^2/2 - \lambda\, d^2\varphi/dz^2$, where the second term is of the same order of magnitude as (and in a few layers even larger than) the first. Indeed, we checked that the numerical value for u in Figure 8b is accurately described by $\varphi^2/2 - (<\varphi> - \varphi)$, where the last term is the discrete version of $\lambda\, d^2\varphi/dz^2$.

As a consequence of the neglect of the nonlocal energy contribution, the approximation $\epsilon + u = \epsilon + (\varphi^l)^2/2$ works also less adequate, as seen in Figure 9 (bottom curves); in this case the approximation *over*estimates $\epsilon + u$ by a factor of around 2 in one or two layers. Hence, we may expect that the GSA equations for $\chi = 0.5$ are more approximate than for $\chi = 0$, and those for intermediate solvencies will be in between. Nevertheless, we will see that most of the trends are still predicted rather well, even for $\chi = 0.5$.

The eigenfunction g is related to the concentration φ^{trl} of train and loop segments (eq 16) and to the concentration φ^{ae} of chain ends (eq 18); as before, we define φ^{trl} as the sum of φ^{tr} and φ^l. Both dependencies can be checked against the full numerical model. Figure 10 shows plots of g, $\sqrt{\varphi^{trl}}$, and $(N/2b)\varphi^{ae}$ for both $\chi = 0$ and $\chi = 0.5$. The lengths p and d needed to compute g and b were obtained from solving eqs 27 and 28, and the quantities φ^{tr}, φ^l, and φ^{ae} were taken from the numerical data. We first compare g and $\sqrt{\varphi^{trl}}$. In the surface layer, there is nearly perfect agreement, which is perhaps not surprising since the discrete version of the boundary condition (eq 28) was used to compute p and d. For large distances the agreement is good, but in the intermediate region (layers 2−4 for $\chi = 0$ and a wider region for $\chi = 0.5$) g is systematically below $\sqrt{\varphi^l}$; the maximum deviation is around 20% for $\chi = 0.5$.

There are several reasons for these differences. The first is that the factor e^u in $\varphi^l = e^u g^2$ was omitted (see above eq 16), which makes the analytical loop concen-

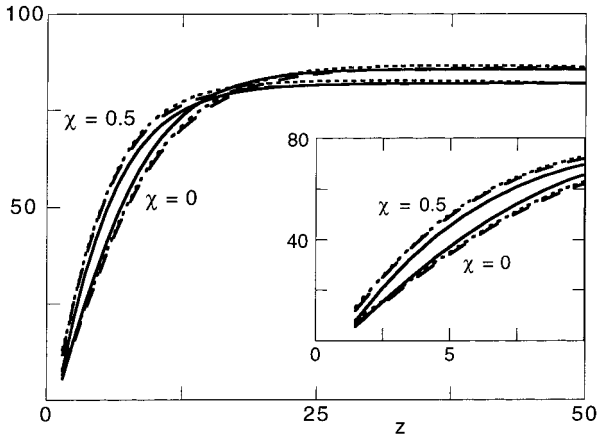

Figure 11. Comparison of the function f (solid curves) with φ^t/φ^{ae} (dotted) and with $\sum_s G^f_{z,s} e^{-\epsilon s}$ (dashed) for $\chi = 0$ and $\chi = 0.5$. The function f is the analytical expression, and φ^t, φ^{ae}, and $G^f_{z,s}$ are numerical SCF results. The inset shows some detail for the inner layers. Conditions as in Figure 10.

tration lower than the numerical one; this effect is more pronounced for $\chi = 0$, where u is relatively large. The second is that the condition that the volume fractions of polymer and solvent should add up to unity is not accounted for in the analytical model (except for the train layer). A third reason is that the continuum version of the second derivative d^2g/dz^2 in eq 17 is for small z smaller than the discrete version $g_{z-1} - 2g_z + g_{z+1}$, which also leads to lower values of g in the continuum model.[22] Finally, for $\chi = 0.5$ the main reason is the neglect of the nonlocal energy contribution, as discussed above. Because of these effects, the analytical model underestimates the contribution of loops and the end-point concentration in these layers: the curves for $(N/2b)\varphi^{ae}$, where φ^{ae} is taken from the numerical data, lie slightly above the curves for g. In the outer layers (not shown in Figure 10) this trend is reversed, since in both models the total number of end points is equal to $2\Gamma/N$, and Γ does not differ much between the two models.

Figure 11 gives a similar comparison for the function f. Its analytical form for $\chi = 0$ and $\chi = 0.5$ (eqs 34 and 38, with values for p and d as described above for g) is compared with the ratio φ^t/φ^{ae} (eq 20a) and with the sum $\sum_s G^f_{z,s} e^{-\epsilon s}$ (eq 21b), where φ^t, φ^{ae}, and $G^f_{z,s}$ were taken from the numerical data and ϵ is the "numerical" value as found from Figure 7. The three curves nearly coincide, indicating that the analytical equations for f are quite adequate to describe tails. Despite the greatly different form of the analytical expressions, there are hardly systematic differences between $\chi = 0$ and $\chi = 0.5$: the initial slope for $\chi = 0.5$ is slightly steeper than for $\chi = 0$, and the final level (which is $1/\epsilon = d^2/\lambda$) is slightly lower.

5.2. Concentration Profiles and Adsorbed Amounts. Figure 12 gives typical profiles for loops and tails in the plateau region ($N = 10^3$, $\varphi^b = 10^{-6}$, $\chi_s = 1$) for both $\chi = 0$ and $\chi = 0.5$. The main figure is with a logarithmic scale for φ^l and φ^t and shows a wide region; the smaller diagrams, with linear scales, give some more details for the inner layers. The full curves are the numerical SCF results; the dotted curves were obtained from $\varphi^l = g^2$ and $\varphi^t = (2b/N)gf$ with $p = 0.598$ and $d = 4.650$ (eqs 27 and 28). The agreement is quite satisfactory. As discussed above, the analytical model underestimates φ^l in the inner layers, and from Figure 12 it is clear that φ^l is overestimated in the periphery of the adsorbed layer, where the effect of free chains was neglected. Tails are described surprisingly well, especially for $\chi = 0$. In a Θ solvent the analytical model slightly underestimates tails, but the effect is only minor.

Figure 12 also provides evidence that z^* is indeed larger than d: the loop and tail profiles cross one another around $z = 10$, twice the distal length d. Also for (much) longer chains $z^* > d$, as z^* is more or less proportional to d. We return to this point in the second paper of this series.

The next three figures give an example of the dependence of the total adsorbed amount Γ on N, on log φ^b, and on χ_s, for conditions similar to those of Figure 4. In this way, the Henry and plateau regions (and the crossover between the two) are covered. Figure 13 shows how, for $\varphi^b = 10^{-25}$ and $\chi_s = 1$, Γ depends on N. For small N the Henry regime applies, where log $\Gamma \propto N$ according to eq 42. For high N, where Γ depends much less on N, we have the plateau region. For $\chi = 0$ the crossover between the two regimes is at $N = 129$, as calculated below eq 44; for $\chi = 0.5$ the crossover is at lower N (around 100), mainly because d_h for $\chi = 0.5$ is smaller (see Figure 5), which according to eq 44 leads to a lower value for N.

The Henry region is shown in the inset of Figure 13, which illustrates that in this case the analytical equations give an accurate description even for very short chains. The slope d log Γ/dN in the Henry region is only a function of χ_s, according to eq 42 (and the text following this equation), and is given by $0.43\lambda/d_h^2$, where d_h equals 0.760 for $\chi = 0$ and 0.680 for $\chi = 0.5$ (see Figure 5). For $N \rightarrow 0$, Γ is of order φ^b because in eq 42a both the prefactor and the exponential factor are of order unity.

As stated above, in the plateau region the effect of the chain length on Γ is much weaker. For $\chi = 0$, Γ reaches a limiting value of order unity; for $\chi = 0.5$, Γ is higher and increases weakly (logarithmically) with the chain length. These aspects will be dealt with in more detail in the second paper of this series. The analytical model underestimates Γ in the plateau region, mainly because loops are underestimated. Hence, this effect is relatively small for $\chi = 0$ (where trains dominate) and relatively more important for $\chi = 0.5$ (where there are more loops and, more importantly, the approximation for $\epsilon + u$ is worse) and amounts to about 15% in the latter case.

Figure 14 gives, for $N = 100$ and $\chi_s = 1$, double-logarithmic adsorption isotherms $\Gamma(\varphi^b)$ in a good solvent ($\chi = 0$) and a Θ solvent. The crossover between the Henry and plateau regimes is for $\chi = 0$ at log $\varphi^b \approx -19.5$, as calculated below eq 44, and for $\chi = 0.5$ it is at lower φ^b because of the lower value of d_h. The Henry parts of the isotherms are well described by $\Gamma = (1 + d_h e^{-0.5/d_h})^2 \varphi^b e^{\lambda N/d_h^2}$, where again $d_h = 0.76$ for $\chi = 0$ and $d_h = 0.68$ for $\chi = 0.5$. Consequently, the slope d log Γ/d log φ^b is unity in this region, and Γ is about 4.5 decades higher for $\chi = 0.5$. The main factor in this ratio is $\exp(\lambda N/d_h^2)$ in eq 42a: $0.43\lambda N(0.68^{-2} - 0.76^{-2}) \approx 4.5$.

On the rough scale used in the main Figure 14, the agreement between the numerical and analytical models looks nearly perfect, in both the Henry and plateau regions. However, plotting the data for the plateau region with a linear scale for Γ (inset Figure 14) shows some systematic (though still small) differences. The

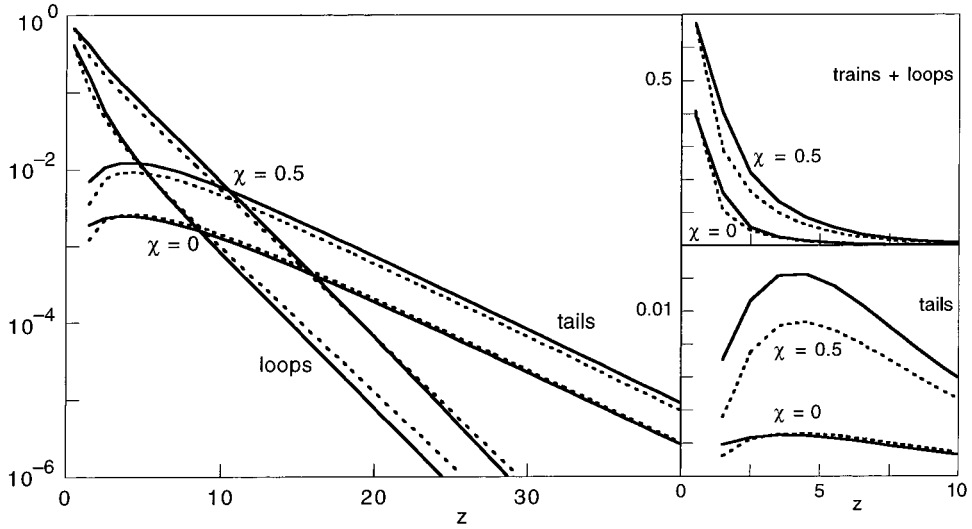

Figure 12. Loop and tail profiles according to the numerical SCF model (solid curves) and according to the analytical approximations (dotted). The main figure is with a logarithmic scale for the volume fractions; the smaller diagrams show, with linear scales, more detail for the inner layers. Conditions as in Figure 10.

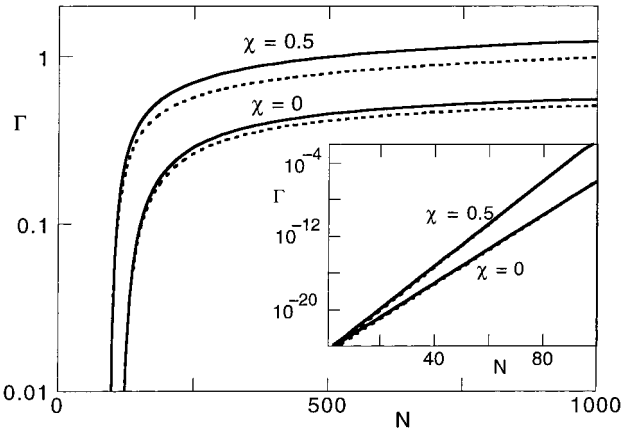

Figure 13. Dependence of the total adsorbed amount Γ on the chain length N according to the numerical SCF model (solid curves) and the analytical approximations (dotted), for $\chi_s = 1$, $\varphi^b = 10^{-25}$, and $\lambda = 1/4$. The inset shows more detail for the Henry region (small N).

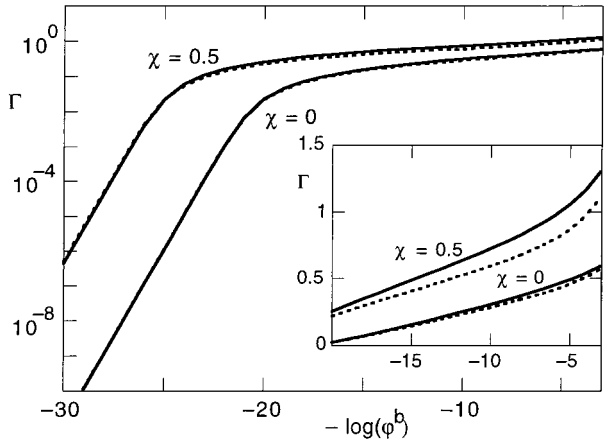

Figure 14. Adsorption isotherms according to the numerical SCF model (solid curves) and the analytical approximations (dotted), for $N = 100$, $\chi_s = 1$, and $\lambda = 1/4$. The main figure is with logarithmic scales for both Γ and φ^b; the inset shows more detail of the plateau region, with a linear scale for Γ.

reason is the same as before: the analytical model underestimates the contribution of loops because of the inaccuracies of g in the layers next to the surface layer

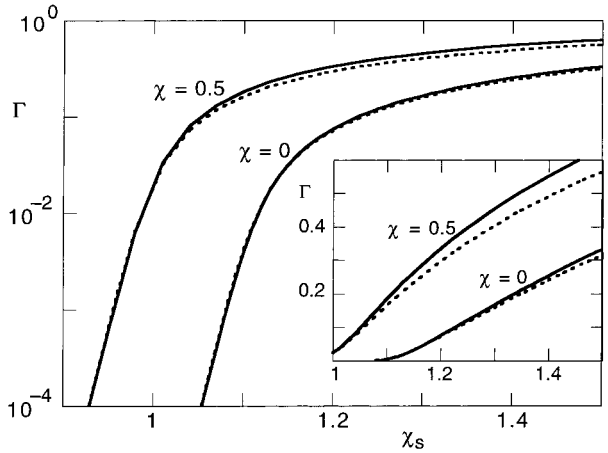

Figure 15. Dependence of the adsorbed amount Γ on the adsorption energy parameter χ_s according to the numerical SCF model (solid curves) and the analytical approximations (dotted), for $N = 100$, $\varphi^b = 10^{-25}$, and $\lambda = 1/4$. The inset shows details of the plateau region with a linear scale for Γ.

(see also Figure 10). For $\chi = 0$, where loops contribute only slightly at this low solution concentration, this effect is small, and for $\chi = 0.5$ it is bigger (but still not more than about 10%), mainly because the approximation in $\epsilon + u$ (see Figure 10) is rather poor. Nevertheless, we may conclude that the analytical model, which uses only two parameters (none of these being free), works surprisingly well.

Figure 15 shows the dependence of Γ on χ_s, for $N = 100$ and $\varphi^b = 10^{-25}$. Again the Henry regions at low χ_s and the plateau regions (higher χ_s) are clearly discernible. The crossover for $\chi = 0$ is at $\chi_s = 1.15$ (see below eq 44); for $\chi = 0.5$ it is lower by an amount $\lambda\chi = 0.125$. Again there is very good agreement between the numerical and analytical models. However, for $\chi_s - \chi_{sc}$ smaller than about 0.1 (not shown in the figure) the analytical model breaks down; under these conditions of very weak adsorption, $\sqrt{N}\Delta\chi_s < 1$, the general ground-state dominance approach is not appropriate (indeed the argument of the exponential in eq 14 is then less than 1 for all segments). Moreover, the approximations $u = \varphi$ or $u = \varphi^2/2$ no longer hold, and the neglect of tails is not allowed for very weak adsorption where

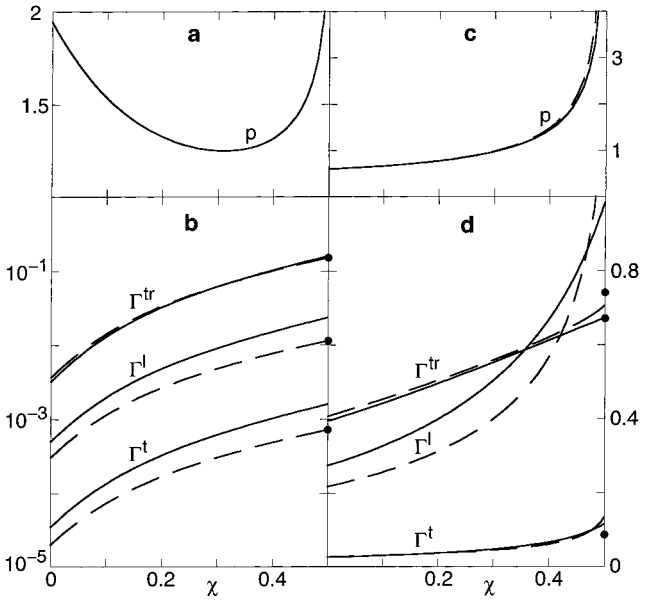

Figure 16. The dependence of the adsorbed amounts in trains (Γ^{tr}), loops (Γ^{l}), and tails (Γ^{t}) (lower diagrams) and that of the parameter p (top) on the solvency. The left-hand-side diagrams are for the same conditions as in Figure 15 for $\chi_s = 1.1$, where there is a crossover from the Henry regime at $\chi = 0$ to the plateau regime at $\chi = 0.5$. To the right a typical plateau-regime situation ($N = 1000$, $\varphi^b = 10^{-6}$, $\chi_s = 1$) is given. In the top diagrams, the full curves were computed with the coupled equations for p and d, and in Figure 16c the dashed curve represents the uncoupled plateau approximation for p (eq 45a). In the bottom diagrams, the solid curves correspond to the numerical SCF model, and the dashed curves to the analytical "good solvent" case; the dots were obtained with the equations for a Θ solvent.

loosely attached coils develop more and longer tails. For strong adsorption, the deviations for $\chi = 0.5$ are somewhat higher than for $\chi = 0$, as in the previous figures.

For high χ_s (outside the range shown in Figure 15) Γ becomes independent of χ_s, as Γ^{tr} approaches unity. The total adsorbed amount for this low φ^b and low N is only slightly higher: tails are negligible under these conditions, and also loops contribute only slightly. Since p is small for $\chi_s \to \infty$, $x_2 \approx 1/d \approx 1/d_0$ (with $d_0 = 0.66$ in this case). Then eq 35b predicts $\Gamma^{l} \approx 0.04$ for $\chi = 0$, and eq 40b gives $\Gamma^{l} \approx 0.06$ for $\chi = 0.5$. Hence, the asymptotic values for Γ at high χ_s are 1.04 and 1.06, respectively, according to the analytical model. The numerical model gives slightly higher values, but in both models the adsorbance goes to a limiting value at high χ_s which, under the conditions of Figure 15, is only slightly above one monolayer. We return to these issues in the following paper, where we consider more realistic values for φ^b and N.

So far, we have only shown results for the two extremes $\chi = 0$ and $\chi = 0.5$. In Figure 16 we consider intermediate solvencies. The left-hand side diagrams in Figure 16 apply to $N = 100$, $\varphi^b = 10^{-25}$, and $\chi_s = 1.1$ and illustrate the effect of changing the solvency along a vertical line in Figure 15 at $\chi_s = 1.1$, where the system crosses over from the end of the Henry regime at $\chi = 0$ to the beginning of the plateau regime at $\chi = 0.5$. Because of this crossover, we cannot use the limiting expressions for the Henry regime or for the plateau regime and have to use the "coupled approximation", solving p and d from the two simultaneous eqs 27 and 28. For this set of parameters, d turns out to be nearly constant: it changes gradually from 0.696 at $\chi = 0$ (which value follows also from eq 41a or 41b) to 0.673 at $\chi = 0.49$. For this entire range in χ the equations for good solvents were used. In contrast, p varies nonmonotonically in this transition region, from 1.945 at $\chi = 0$ to a minimum value 1.249 at $\chi = 0.31$ to 1.964 at $\chi = 0.49$, as shown in Figure 16a. With these values of p and d, the adsorbed amounts Γ^{tr}, Γ^{l}, and Γ^{t} in trains, loops, and tails are easily calculated (dashed curves in Figure 16b). The solid curves in Figure 16b are the numerical data, and the dots at $\chi = 0.5$ are the analytical results for a Θ solvent. In this case of weak adsorption, the adsorbance is dominated by the trains. The values of Γ^{tr} at $\chi = 0$ and $\chi = 0.5$ in Figure 16b are thus nearly the same as those for Γ in Figure 15. As expected, all three contributions to Γ increase monotonically with χ. The agreement between the analytical and the numerical model in Figure 16b is excellent for trains and quite reasonable for loops and tails.

The nonmonotonic behavior of p (Figure 16a) can be understood as follows. The train density is proportional to $v^{-1} \sinh^{-2}(p_1/d)$, where d in this case is essentially a constant. For small χ, $v = 1 - 2\chi$ is nearly constant, and in order to find an increasing Γ^{tr} with increasing χ the parameter p_1 ($= p + {}^1/_2$) has to decrease. As the system crosses over to the plateau region (χ closer to 0.5), p_1 increases again. Well into the plateau region, this increase is roughly as $1/\sqrt{v}$ (see Figure 6 and eq 45a), but in Figure 16a it is still weaker, such that v^{-1} increases more strongly than $\sinh^{-2}(p_1/d)$ decreases.

In Figure 16b, the analytical equations for good solvents, based upon dominance of the linear tem $v\varphi$ (second virial) in eq 13 over the quadratic term $\varphi^2/2$ (third virial), work well up to $\chi = 0.49$ ($v = 0.02$); there is hardly a discontinuity visible between the dashed curves (which nevertheless diverge for $v \to 0$; not indicated in Figure 16b) and the dots for the Θ result (based upon the third virial only). This is because the concentrations in the loop region are quite low in this case of weak adsorption. For relatively high χ, this second-virial dominance does not hold in the train layer, but here we do not use an expansion: in the boundary condition the full Flory−Huggins field is accounted for.

The right-hand-side diagrams in Figure 16 give analogous results for the plateau regime and longer chains ($N = 1000$, $\varphi^b = 10^{-6}$, $\chi_s = 1$). In Figure 16d, where now a linear scale is used for Γ, the analytical model is quite accurate for trains and tails, and the loop contribution is somewhat underestimated, as discussed before. In this case d ($\approx R/y$) is again nearly constant, decreasing from 4.624 at $\chi = 0$ to 4.520 at $\chi = 0.5$. Now p is smaller than d, and it increases monotonically with increasing χ, as expected. For $\chi \lesssim 0.4$ the uncoupled plateau approximation (eq 45a) gives basically the same results as the coupled eqs 27 and 28. Only for higher χ does the plateau approximation (dashed curve in Figure 16c) become inaccurate, as the condition $p \ll d$ no longer applies. For χ close to 0.5, the coupled equations have thus to be used to find p.

In this range of χ there is another reason which restricts the validity of the present analytical model. As the loop density increases in the region adjoining the trains, the second-virial dominance no longer holds for small v. Indeed, in Figure 16d a discontinuity is now seen between the dashed curves (which diverge for $\chi \to 0.5$, as can be seen clearly for loops) and the Θ results. Nevertheless, the analytical model is quite adequate up

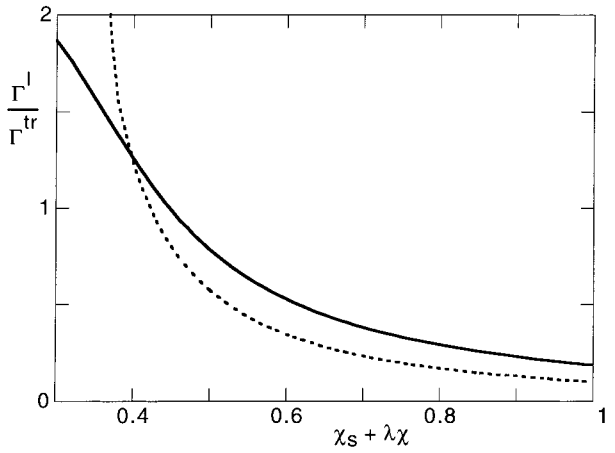

Figure 17. The ratio between the adsorbance in loops and trains in the Henry region according to the numerical SCF model (solid curve) and the analytical approximations (dotted), for conditions as in Figure 15. The two sets of data for a good solvent and for a Θ solvent exactly coincide when plotted as a function of $\chi_s + \lambda\chi$, for both models.

to $\chi \approx 0.47$, because the concentration φ_2 in the second layer usually does not exceed 0.3, even for strong adsorption.

Except for Figure 16, we have presented in this paper the total adsorbed amount without specifying the contributions of trains, loops, and tails. For the plateau region we will address these issues in the next paper. The Henry region is less interesting, and certainly less relevant from an experimental point of view, and will not be treated in this second paper. However, in section 4.3.1 we derived some simple equations for the Henry regime, assuming that tails may be neglected. The ratio Γ^{l}/Γ^{tr} ($= I_{gg}/g_1^2$) was found to be given by $(d_h/2)e^{-1/d_h}$, which is only a function of χ_s.

Figure 17 compares this dependence with the numerical data for the Henry regime, for both $\chi = 0$ and $\chi = 0.5$. The solid curve gives the two sets of SCF data, which fall exactly on top of each other. The same applies for the dotted curve, which gives the function $(d_h/2)e^{-1/d_h}$, where d_h is the same at equal $\chi_s + \lambda\chi$ (compare Figure 5). The simple equation used here for Γ^{l}/Γ^{tr} gives the same result as the solution of the coupled eqs 27 and 28. Although the analytical model underestimates the contribution of loops, the trends in both models for the ratio Γ^{l}/Γ^{tr} are the same: trains become dominant and loops less important as χ_s increases. For small χ_s the analytical model breaks down, as discussed in connection with Figure 15. For $\chi_s - \chi_{sc}$ larger than about 0.1, the agreement between the two models is quite satisfactory.

6. Conclusions

We presented an explicit analytical mean-field calculation for homopolymer adsorption from dilute solution, constructed to approximate the full numerical self-consistent lattice theory of Scheutjens and Fleer. Our treatment is based upon the expansion for long chains as introduced by Semenov et al.[13] As in the original theory, the end-point distribution of adsorbed chains is calculated in the ground-state approximation (GSA). If contributions of free states to this distribution are neglected, the theory is self-consistent only when tail monomers are neglected in the adsorbance. Here we adopt the slightly more accurate version where contributions beyond the ground state are accounted for to lowest order.[13,14] This procedure entails an additional constant (called b in this paper) which is determined by the self-consistency requirement (this constraint is not automatically satisfied in the perturbative scheme).

For a Θ solvent a simple rescaling of the ground-state eigenfunction is not enough to account for free state contributions to the loop monomer density. A calculation based upon the rest function as introduced before[13,14] is in principle more accurate. We did such a calculation. However, the agreement with the numerics does not improve. The discrepancy, which typically amounts to some 10%, remains. The main reason is the neglect of nonlocal energy effects (i.e., the contribution of the second derivative of $\varphi(z)$ to the local field u) in the continuum theory, which is of no consequence for $\chi = 0$ but is important for χ unequal to zero. There is no easy way to incorporate this effect in the analytical treatment.[25]

The introduction of the end-point density distribution for free chain sections allows to explicitly account for tails. In its general form, the theory produces a set of two coupled nonlinear differential equations that can only be discussed in terms of asymptotics or solved numerically. However, for moderate chain lengths (up to around $N = 10^4$, as often encountered in experiments) and for dilute solutions the equations can be approximately decoupled and solved in closed form. In those cases the sum $\epsilon + u$ in the differential equation for the ground-state eigenfunction g ($-\epsilon$ being the ground-state eigenvalue) may be replaced by ϵ in the periphery of the layer (which is equivalent to stating that the crossover distance z^* between loop and tail regimes is larger than the distal length $d = \sqrt{\lambda/\epsilon}$). This approximation breaks down for very large N, because then ϵ is very small (hence, d is very large).

There are two constants to be determined from the boundary condition at the wall and the self-consistency requirement. We choose the extrapolation length, which is the decay length very close to the surface, and the distal length, which is the exponential decay length in the dilute periphery of the layer. In the undersaturated Henry regime, the two length scales merge into one, and only one parameter d, which is then only a function of χ_s, is needed to describe the exponentially decaying profile.

To make contact with the Scheutjens−Fleer lattice theory, we adopt a discrete description of the lattice layer closest to the wall (the train layer), but we maintain a continuum description further away from the surface (i.e., for loops and tails); in this region the concentration profiles vary fairly smoothly, even for strong adsorption. The resulting boundary condition is different from that used so far in continuum descriptions. It introduces a (nonuniversal) adsorption threshold and allows to account for a high density in the train layer, whereas elsewhere in the layer the interaction is expanded in the local density. As a result, analytical approximations to the numerical lattice theory are obtained with an accuracy of order of (or better than) 10%.

All the approximations made in the analytical theory (GSA, density expansion of the interaction, decoupling of the differential equations, etc.) are carefully checked against the numerical data over a wide range of parameters. The remaining minor discrepancies mainly come from the inner part of the loop layer, where the profiles are not entirely smooth over the step length.

In a Θ solvent the neglect of nonlocal energy effects forms the most important reason for the (still relatively small) differences between the analytical and numerical models.

In this paper we did most of the calculations for two extremes in solvency: $\chi = 0$ and $\chi = 0.5$. The former limit is rather academic, as in experimental good solvents χ is usually in the range 0.4−0.45 ($v = 0.1-0.2$). This is the range where our treatment for good solvents is still appropriate, because in the loop and tail region the second virial contribution ($v\varphi$) still dominates the third ($w\varphi^2$). (Clearly, this does not apply for the trains, but here we use the full Flory expression $-2\chi\varphi - \ln(1-\varphi)$ in the boundary condition). For solvency conditions closer to the Θ point (sometimes called tricritical solvents) our present analytical model breaks down for strong adsorption (even though under most conditions it works well up to $\chi \approx 0.47$). It is, in principle, possible to improve the treatment for the tricritical range.[26]

Another problem is that the mean-field model neglects the swelling of the adsorbed layer and of chains in the bulk solution, which would make our treatment inadequate for good solvents. In the concluding remarks of the second paper we will argue that for experimental good solvents (χ in the range 0.4−0.45) and moderately long chains the swelling in the layer is not important and that the swelling in the bulk solution can be accounted for by renormalizing the solution concentration.

The general continuum theory has recently been extended to polymers with various architectures.[21] Following the same lines one could try to write solutions in closed form that reproduce the numerical lattice results for such more complex systems. Before attempting such an undertaking, in the second paper of this series we will calculate several physical quantities for homopolymers over a wide range of parameters, for conditions which are relevant for typical experimental systems.

Acknowledgment. The authors express their admiration for the late Jan Scheutjens, who not only developed the lattice model but was also always trying to find analytical approximations to his numerical data. He would definitely have appreciated the present progress in the analytical theory.

Appendix I. List of Most Important Symbols

The abbreviations (g) and (t) in this list stand for a good and a Θ solvent, respectively. When two symbols are given for the same quantity, the first [with subscript-(s)] is for the lattice version and the second (with arguments) for the continuum variant.

Glossary

Superscripts:

a	adsorbed chains
ae	end segments of adsorbed chains
b	bulk solution
e	end segments (all chains)
f	free chains
l	loops
t	tails
tr	trains
trl	trains and loops

a	bond length
b	constant related to ϵ through $b^2 = \varphi^b e^{\epsilon N}$ (eq 12)
b_0	approximation for b in the plateau region: eq 46 (g), eq 48 (t)
d	exponential decay length, related to ϵ through $\epsilon = \lambda/d^2$ (eq 30a); in the plateau region d is the distal length
d_0	first-order estimate for d, related to ϵ_0 through $\epsilon_0 = \lambda/d_0^2$; also, $d_0 = \sqrt{\lambda N}/y$ (eq 30)
d_h	exponential decay length in the Henry region
d_p	distal length (exponential decay length) in the plateau region
f_z, $f(z)$	function used to describe tails, the concentration of which is proportional to fg
$F(x)$	function needed for f in a Θ solvent (eq 38b, Figure 3)
g_z, $g(z)$	renormalized ground-state eigenfunction $b\psi(z)$
g_1	value of g in the train layer: $g_1 = g(1/2)$
g_2	value of g in the second layer: $g_2 = g(3/2)$
G_z, $G(z)$	segmental weighting factor: $G_z = e^{-u_z}$, $G(z) = e^{-u(z)}$
$G_{z,s}$, $G(z,s)$	statistical weight for walks of s segments to end in z (end-point distribution)
G_N^a	statistical weight $= \sum_z G_{z,N}^a$ for adsorbed chains; it equals Γ/φ^b (eq 9)
I	$\int_0^\infty (\gamma/\sinh x)\,dx = 0.733$ (g), or $\int_0^\infty (\gamma/\sqrt{\sinh 2x})\,dx = 0.606$ (t)
$I(x_2)$	similar to I, but with lower bound x_2 and γ replaced by $\gamma - \gamma_2$
I_g	integral over g in the tail/loop region: $I_g = \int_1^\infty g\,dz = d\int_{x_2}^\infty g\,dx$; the adsorbance Γ equals $b(g_1 + I_g)$ (eq 19)
I_{gg}	as I_g, with g replaced by g^2; I_{gg} equals Γ^l, the adsorbance in loops
I_{gf}	as I_g, with g replaced by gf; I_{gf} equals $(N/2b)\Gamma^t$, where Γ^t is the adsorbance in tails
K	numerical constant 1.854 [$=F(\infty)$]
l	lattice spacing, related to the bond length a through $l = a/\sqrt{6\lambda}$
N	number of segments per chain
p	integration constant; in the plateau regime it is the proximal length
p_i	abbreviation for $p + i/2$; $p_1 = p + 1/2$, $p_2 = p + 1$, and $p_3 = p + 3/2$ occur in the equations
p_h	value of p in the Henry region
p_p	proximal length in the plateau region
p_∞	proximal length for $\chi_s \rightarrow \infty$
q	constant related to the lattice type: $q = \sqrt{2\lambda}$ (g), $q = \sqrt{6\lambda}/2$ (t)
R	radius of gyration: $R^2 = \lambda N$
$R_{z,s}$	ratio $G_{z,s+1}^a/G_{z,s}^a$
s	segment ranking number: integer 1,2, ..., N (lattice) or continuous variable from 0 to N
$S(x)$	function defined in eq 34a, used for describing γ and f in a good solvent
$T(x)$	function defined in eq 38a, used for describing γ and f in a Θ solvent
u_z, $u(z)$	SCF field at position z
v	excluded-volume parameter $1 - 2\chi$
x	reduced distance from the surface: $x = (z + p)/d$
x_i	$x_i = p_i/d = (p + i/2)/d$; x_1 is the value of x at $z = 1/2$, x_2 that at $z = 1$, and x_3 that at $z = 3/2$

y	concentration parameter, defined by $y^2 = \ln(1/\varphi^b)$
z	distance from the wall (continuum); layer number (lattice); the center of the lattice layers is at a distance $z - {}^1/_2$ from the wall (which is at $z = 0$ in the continuum)
z^*	crossover distance where $\varphi^l = \varphi^t$
α	power-law exponent in $\xi \propto \varphi^{-\alpha}$ or $\varphi \propto z^{-1/\alpha}$: in a Θ solvent $\alpha = 1$, and in a good solvent $\alpha = {}^1/_2$ (mean field) or ${}^3/_4$ (excluded-volume correlations)
$\gamma(x)$	function used to describe f. It is defined in eq 33 (g) and eq 37 (t) and plotted in Figure 2
$\gamma_2(x)$	function defined in eq 33 (g) and eq 37 (t). The function f is proportional to $\gamma - \gamma_2$
Γ	adsorbance: $\Gamma = b(g_1 + I_g)$, $\Gamma^{tr} = g_1^2$, $\Gamma^I = I_{gg}$, $\Gamma^t = (2b/N)I_{gf}$
ϵ	minus the ground-state eigenvalue. It is related to d through $\epsilon = \lambda/d^2$; also, $\epsilon = \epsilon_0 + (2/N)\ln b$ (eq 12)
ϵ_0	first-order estimate for ϵ: $\epsilon_0 = y^2/N = N^{-1}\ln(1/\varphi^b)$ (eq 12)
$\kappa(x)$	function needed for f in a good solvent; it is defined in eq 34b
λ	lattice parameter (${}^1/_6$ in a cubic lattice, ${}^1/_4$ in a hexagonal lattice)
λ_0	$1 - 2\lambda$
ξ	correlation length of concentration fluctuations
φ_z, $\varphi(z)$	segment concentration at position z
$<\varphi_z>$	$\varphi_z + \lambda(\varphi_{z-1} - 2\varphi_z + \varphi_{z+1}) \approx \varphi + \lambda\, d^2\varphi/dz^2$
φ^b	bulk solution concentration: $\varphi^b = \varphi_\infty = \varphi(\infty)$
$\varphi_{z,s}$, $\varphi(z,s)$	contribution to φ_z, $\varphi(z)$ due to segment s
χ	Flory−Huggins interaction parameter (0 in a good solvent, 0.5 in a Θ solvent)
χ_s	adsorption energy parameter
χ_{sc}	value of χ_s at the adsorption/desorption transition: $\chi_{sc} = -\ln(1 - \lambda) - \lambda\chi$
$\psi(z)$	ground-state eigenfunction

References and Notes

(1) Napper, D. H. *Polymer Stabilisation of Colloidal Dispersions*; Academic Press: London, 1983.
(2) Fleer, G. J.; Cohen Stuart, M. A.; Scheutjens, J. M. H. M.; Cosgrove, T.; Vincent B. *Polymers at Interfaces*; Chapman and Hall: London, 1993.
(3) Scheutjens, J. M. H. M.; Fleer, G. J. *J. Phys. Chem.* **1979,** *83*, 1619.
(4) Scheutjens, J. M. H. M.; Fleer G. J. *J. Phys. Chem.* **1980,** *84*, 178.
(5) Ploehn, H. J.; Russel, W. B.; Hall, C. K. *Macromolecules* **1988**, *21*, 1075.
(6) Ploehn, H. J.; Russel, W. B. *Macromolecules* **1989**, *22*, 266.
(7) De Gennes, P. G. *Adv. Colloid Interface Sci.* **1987**, *27*, 719.
(8) Van der Linden, C. C.; Leermakers, F. A. M. *Macromolecules* **1992**, *29*, 3449.
(9) Eisenriegler, E. *Polymers near Interfaces*; World Scientific: Singapore, 1993.
(10) Semenov, A. N.; Joanny, J. F. *Europhys. Lett.* **1995**, *29*, 279.
(11) Aubouy, M.; Guiselin, O.; Raphael E. *Macromolecules* **1996**, *29*, 7261.
(12) Johner, A.; Bonet-Avalos, J.; Van der Linden, C. C.; Semenov, A. N.; Joanny, J. F. *Macromolecules* **1996**, *29*, 3629.
(13) Semenov, A. N.; Bonet-Avalos, J.; Johner, A.; Joanny, J. F. *Macromolecules* 1**996**, *29*, 2179.
(14) Semenov, A. N.; Joanny, J. F.; Johner, A. In *Theoretical and Mathematical Models in Polymer Research*; Grosberg, A., Ed.; Academic Press: San Diego, 1998.
(15) Helfand, E. *J. Phys. Chem.* **1975**, *62*, 999.
(16) Hong, K. M.; Noolandi, J. *Macromolecules* **1981**, *14*, 727.
(17) De Gennes, P. G. *Macromolecules* **1981**, *14*, 1637.
(18) Abramowitz, M.; Stegun, I. A. *Handbook of Mathematical Functions*, 5th ed.; New York, 1968.
(19) Bouchaud, E.; Daoud M. *J. Phys. (Paris)* **1987**, *48*, 1991.
(20) Gorbunov, A. A.; Skvortsov, A. M.*Vysokomol. Soed.* **1989**, *31*, 1224.
(21) Rubin, R. J. *J. Chem. Phys.* **1965**, *43*, 2392.
(22) Fleer, G. J.; Leermakers F. A. M. 6th Dresden Polymer Discussion 1997; *Macromol. Symp.* **1997**, *126*, 65.
(23) Joanny, J. F.; Johner A. *J. Phys. II (Paris)* **1996**, *6*, 511.

(24) This is the usual energy term retained for simple (monomeric) liquids, where it accounts for the finite range of the interactions to lowest order. The lattice model produces a similar term, but here it is rather an effect of the finite monomer size; hence, the prefactor is simply χ. In polymeric liquids there is an additional entropy contribution due to chain elasticity (induced by chain connectivity) which is accounted for in both the lattice and analytical theories. This entropy contribution is proportional to $1/\varphi$ and thus dominates, except in a few layers close to the surface.

(25) It would, for example, be possible to include those effects in the standard square gradient theory, only accounting for loops, by defining a function $\psi \equiv \sqrt{\varphi(\varphi + 1)} + \ln(\sqrt{\varphi} + \sqrt{(\varphi+1)})$. Now the square gradient of ψ equals $1 + 1/\varphi$ times the square gradient of φ, so that both the energetic and elastic nonlocal contributions are generated. The corrections to the leading $1/\varphi$ term are only important in the inner layers.

(26) In principle, the mean-field ground-state equation can be solved using $u = v\varphi + w\varphi^2$, which then would give rather complicated expressions. It is even possible to solve the equation formally for an arbitrary free energy density (such as the full Flory−Huggins expression as used in the numerical model) to obtain the function $z(g)$. The equation for the function f (or for the rest function r) then yields formally $f(g)$ (or $r(g)$). Though for a specific case the determination of the integration constants may be tedious, this procedure is in principle straightforward. In each case one should evaluate the free state contribution to the loop concentration and check whether it is negligible or one should use the rest function formalism throughout.

MA980793Y